

Enhancing Long-Term Vegetation Monitoring in Australia: A New Approach for Harmonising and Gap-Filling AVHRR and MODIS NDVI

5 Chad. A. Burton¹, Sami. W. Rifai², Luigi. J. Renzullo³ and Albert. I.J.M. Van Dijk¹

¹ Fenner School of Environment & Society, Australian National University, Canberra, ACT, Australia.

² School of Biological Sciences, The University of Adelaide, Adelaide SA, Australia.

³ Bureau of Meteorology, Hydrology Science, Canberra, Australia

10

Correspondence: Chad Burton (chad.burton@anu.edu.au)

Abstract.

Long-term, reliable datasets of satellite-based vegetation condition are essential for understanding
15 terrestrial ecosystem responses to global environmental change, particularly in Australia which is
characterised by diverse ecosystems and strong interannual climate variability. We comprehensively
evaluate several existing global AVHRR NDVI products for their suitability for long-term vegetation
monitoring in Australia. Comparisons with MODIS NDVI highlight significant deficiencies, particularly
over densely vegetated regions. Moreover, all the assessed products failed to adequately reproduce inter-
20 annual variability in the pre-MODIS era as indicated by Landsat NDVI anomalies. To address these
limitations, we propose a new approach to calibrating and harmonising NOAA's Climate Data Record
AVHRR NDVI to MODIS MCD43A4 NDVI for Australia using a gradient-boosting decision tree
ensemble method. Two versions of the datasets are developed, one incorporating climate data in the
predictors ('AusENDVI-clim': **Australian Empirical NDVI-climate**) and another independent of climate
25 data ('AusENDVI-noclim'). These datasets, spanning 1982-2013 at a spatial resolution of 0.05° and
monthly time step, exhibit strong correlation ($r^2 = 0.89-0.94$) and low relative-mean errors compared to
MODIS MCD43A4 NDVI (MAE = 0.014-0.028, RMSE = 0.021-0.046), accurately reproducing seasonal
cycles over densely vegetated regions. Furthermore, they closely replicate the interannual variability in

Formatted: Superscript

vegetation condition in the pre-MODIS era. A reliable method for gap-filling the AusENDVI record is
30 also developed that leverages climate, atmospheric CO₂ concentration, and woody cover fraction
predictors. The resulting synthetic NDVI dataset shows excellent agreement with observations ($r^2 = 0.82$ -
0.95, MAE = 0.016-0.029, RMSE = 0.039-0.041). Finally, we provide a complete 41-year dataset where
gap filled AusENDVI from January 1982 to February 2000 is seamlessly joined with MODIS [MCD43A4](#)
NDVI from March 2000 to December 2022. Analysing 40-year per-pixel trends in Australia's annual
35 maximum NDVI revealed increasing values across most of the continent. Moreover, Sshifts in the timing
of annual peak NDVI are also identified, underscoring the dataset's potential to address crucial questions
regarding changing vegetation phenology and its drivers. The AusENDVI dataset can be used for
studying Australia's changing vegetation dynamics and downstream impacts on terrestrial carbon and
water cycles, and provides a reliable foundation for further research into the drivers of vegetation change.
40 AusENDVI is open access and available at <https://doi.org/10.5281/zenodo.10802704> (Burton, 2024)

Formatted: Superscript

1 Introduction

Australia is undergoing long-term changes to its climate that are impacting terrestrial vegetation, with
attendant serious implications for ecosystem functioning, carbon and water cycles, and agriculture
(Hoffmann et al., 2019; Canadell et al., 2021; Head et al., 2014; Hughes, 2011; Steffen et al., 2011; Rifai
45 et al., 2022; Ukkola et al., 2016; Donohue et al., 2009). Long-term, reliable datasets that chart the land
surface response to climate change are crucial if we are to identify, understand, and respond to ongoing
terrestrial ecosystem change (Giglio and Roy, 2020; Piao et al., 2019). One of the primary means Earth
System Science has to trace long-term vegetation change is the Normalised Difference Vegetation Index
(NDVI), a widely used satellite-derived indicator of vegetation condition owing to its close relation to
50 vegetation productivity. NDVI provides an efficient means for mapping and monitoring vegetation
condition at continental scales. In Australia, the need for very long records of NDVI to understand change
is amplified by strong variability at both interannual and interdecadal time scales, and ecosystems that are
often driven by periodic, but non-seasonal phenological drivers (Moore et al., 2016; Chambers et al.,
2013; Ma et al., 2013; Beringer et al., 2022).

55 The MODerate resolution Imaging Spectroradiometer (MODIS) NDVI record ($NDVI_{MODIS}$) is generally considered the most reliable global scale dataset due to its high quality radiometrics and accurate georeferencing. Unfortunately, the MODIS record only begins in March 2000 (Vermote et al., 2002). The Advanced Very High-Resolution Radiometer (AVHRR) NDVI record ($NDVI_{AVHRR}$) is the longest contiguous series of satellite data, starting in July 1981, but has several well-known problems owing to a
60 lack of on-board calibration for visible wavelengths, sensor orbital drift, and sensor degradation, making it unreliable for detecting relatively subtle trends over multiple decades (Tucker et al., 2005; Privette et al., 1995; Gorman and McGregor, 1994). Several prominent global $NDVI_{AVHRR}$ products attempt to ameliorate these issues. For example, the Global Inventory Modelling and Mapping Studies version 3 ($NDVI_{GIMMS3g}$) applies Bayesian analysis with Sea-Viewing Wide Field-of-View Sensor NDVI as
65 evidence information to reduce sensor transition discontinuities and increase the dynamic range of $NDVI_{AVHRR}$ (Pinzon and Tucker, 2014), while the NOAA Climate Data Record ($NDVI_{CDR}$) applies a suite of corrections to create a consistent surface reflectance product (Franch et al., 2017), among others (Table 1). However, despite substantial progress, errors and biases in these NDVI products have led to inconsistent findings on global greening (Wang et al., 2022; Wang et al., 2021; Cortés et al., 2021; Frankenberg et al., 2021; Fensholt and Proud, 2012), discrepancies in vegetation seasonality between
70 datasets (Ye et al., 2021), and persistent temporal inconsistencies (Tian et al., 2015; Giglio and Roy, 2020). Recently, Li et al. (2023) developed a new global $NDVI_{AVHRR}$ product, ‘GIMMS-PKU’ ($NDVI_{GIMMS-PKU}$), which effectively calibrates the $NDVI_{GIMMS3g}$ archive to the Landsat record using machine learning techniques, and ‘GIMMS-PKU-consolidated’ ($NDVI_{PKU-consolidated}$) which harmonises
75 $NDVI_{GIMMS-PKU}$ to $NDVI_{MODIS}$ (Table 1), but which has yet to be extensively assessed in the literature (Li et al., 2023).

As much as possible, any NDVI product that exploits the AVHRR and MODIS record to acquire an accurate >40-year record of vegetation condition should attempt to integrate the two seamlessly, while also performing well in the pre-MODIS AVHRR era (1982-2000). Performance should be judged on
80 how well seasonal cycles are represented along with interannual and interdecadal variability, as both seasonal and longer-term fluctuations in vegetation conditions have important ramifications for carbon and water cycles (Ma et al., 2015). An effectively calibrated, harmonised, and gap-filled dataset can form

the basis for studying the biogeophysical impacts of global change and meteorological variability on Australia's terrestrial vegetation. With that in mind, the objectives of this study are as follows:

- 85 • To investigate existing NDVI_{AVHRR} datasets to determine their suitability for long-term vegetation monitoring in Australia by both comparing their consistency with NDVI_{MODIS} during the 2000-2013 overlap period, and with Landsat NDVI (NDVI_{Landsat}) anomalies from 1988-2000.
- 90 • Having established limitations with the existing datasets, calibrate and harmonise NDVI_{AVHRR} to NDVI_{MODIS} solely over Australia at the highest spatial resolution possible. The final dataset should contain the harmonised NDVI_{AVHRR} from January 1982 to February 2000, where it seamlessly joins with the superior NDVI_{MODIS} timeseries, resulting in a reliable 419-year record of vegetation condition for Australia. We will call this time series "AusENDVI" (for Australian Empirical NDVI; NDVI_{AusE})
- 95 • To develop a reliable method for gap filling the NDVI_{AusE} record caused by sensor transitions issues and long periods of missing or suspect data acquisition.
- To demonstrate the utility of this new dataset by exploring NDVI phenology trend analysis, including long-term trends in the value and timing of annual maximum NDVI across the Australian continent.

2 Materials and Methods

100 2.1 Datasets

~~Features-Specifications~~ of all datasets used for either the intercomparison of NDVI products or in the modelling framework are listed in Table 1. For comparisons between NDVI datasets, finer resolution datasets were resampled to match the coarsest grid (i.e., GIMMS, 1/12° or ~8 km over Australia). ~~using Averaging resampling techniques were used for downsampling finer-resolution datasets, while or nearest-neighbour techniques were used when datasets have a similar spatial resolution but either different projections or slightly different grid extents.~~ Wherever datasets are compared, data gaps are matched between all datasets by creating a mask that identifies all missing pixels, and then that common mask is applied to every dataset. This ensures a fair and valid comparison. We chose Landsat's TM and ETM+

(Table 1) as the sensor for comparison in the pre-MODIS era owing to the international efforts to produce a relatively high geometric and radiometric accuracy for its generation, and its lack of sensor transitions
110 [in the pre-MODIS era from 1982-1999](#) (Beck et al., 2011). The chosen surface reflectance Landsat product, Digital Earth Australia's ([DEA](#)) Landsat NBAR (Nadir-corrected BRDF Adjusted Reflectance, where BRDF stands for Bidirectional reflectance distribution function) product is calibrated to Australia's environment using the MODTRAN 4 radiative transfer model and BRDF shape functions derived from
115 MODIS (Li et al., 2010; Byrne et al., 2024).

For the development of the Australian NDVI dataset, we relied on the NOAA NDVI_{CDR} product (Franch et al., 2017) as the input dataset. This was principally because of its higher spatial resolution than the other datasets (~5 km), its lack of gap filling, extensive atmospheric corrections, and its BRDF-based correction of view-angle effects (Ma et al., 2019). As the target dataset, we derived NDVI from the
120 MODIS MCD43A4 surface reflectance NBAR product (NDVI_{MCD43A4}). This reflectance product was chosen because of its similar set of atmospheric corrections when compared with NDVI_{CDR} and [DEA's](#) Landsat NBAR, and its use of both the Terra and Aqua instruments which extends its temporal extent back to March 2000 (Schaaf and Wang, 2015).

All additional input data used in NDVI estimation were temporally aggregated to monthly values
125 by calculating medians and spatially reprojected onto a common 0.05° geographic grid. In addition to filtering based on the quality assurance band ([we filtered for clouds, cloud shadows, and invalid BRDF and channel values](#)) additional criteria were applied to minimise the impact of temporal discontinuities in the NDVI_{CDR} record that may arise from orbital decay or sensor degradation. Monthly NDVI_{CDR} values based on fewer than two observations per month were discarded, along with any values for which the
130 coefficient of variation in daily retrievals for a given month was greater than 50 %. Anomalies in NDVI, solar-zenith-angle, and time-of-acquisition that were greater than 3.5 standard deviations were also discarded (based on a 1982-2013 climatology). Following the advice of Tian et al. (2015), data for several problematic sensor transition periods were discarded (September 1984 - April 1985, July 1988 - September 1989, and July 1993 - December 1994). After filtering, the continental average fraction of
135 available data is 0.79, meaning on average 79 % of the monthly time-steps between 1982-2013 are preserved (Fig. A1).

Table 1: Details of the datasets used in, and produced by, this study.

Dataset & Abbreviation	Native spatial resolution; temporal resolution & range ; additional details	Data Source & Reference
AVHRR Climate Data Record NDVI and Surface Reflectance; NDVICDR	0.05°, Daily , January 1982 to December 2013. Surface reflectance product used for the time-of-day and solar zenith angle.	Version 5, downloaded from Google Earth Engine, (Franch et al., 2017)
MODIS MCD43A4 NDVI; NDVIMCD43A4	~500m, 16-day , March 2000 to December 2022. Calculated from the combined Terra and Aqua MCD43A4 surface reflectance NBAR product.	Version 6.1 downloaded from Google Earth Engine (Schaaf and Wang, 2015)
AVHRR GIMMS3g NDVI; NDVIGIMMS3g	1/12°, Half-month , 1982-2013. AVHRR NDVI with sensor transition discontinuities reduced with Bayesian analysis.	Version 1.0 downloaded from Google Earth Engine (Pinzon and Tucker, 2014)
AVHRR GIMMS PKU NDVI; NDVIPKU, NDVIPKU-consolidated	1/12°, Half-month , 1982-2022. Two variations, ‘GIMMS-PKU-solely’ and ‘GIMMS-PKU-consolidated’, the latter is harmonised with MODIS MOD13C1 . For GIMMS-PKU-solely we loaded pixels labelled as ‘good-quality AVHRR’. For GIMMS-PKU-consolidated we loaded pixels labelled as ‘good-quality AVHRR’ and ‘good-quality MODIS’ and where the harmonisation was run by the random-forest model	Version 1.2 downloaded from https://zenodo.org/records/8253971 (Li et al., 2023)
Digital Earth Australia’s Landsat NDVI (NBAR); NDVILandsat	30m, 8-day , 1987-2012, NDVI calculated from an Australian-specific Landsat 5 & 7 surface reflectance NBAR product.	Collection 3, https://docs.dea.ga.gov.au/data/product/dea-surface-reflectance-nbar-landsat-5-tm/ (Li et al., 2010)
AusENDVI-clim and AusENDVI-noclim; NDVIAusE-clim, NDVIAusE-noclim	0.05°, Monthly , 1982-2013. Calibrated and harmonised NDVI for Australia using machine-learning techniques. The ‘clim’ version of the dataset includes climate variables in the feature set, the ‘noclim’ version does not.	This study
Synthetic NDVI; NDVISYN	0.05°, Monthly , 1982-2022. A machine-learning derived synthetic NDVI built using climate, CO ₂ , and landscape features, and trained on NDVIAusE-clim and NDVIMCD43A4.	This study

ANU Climate: <ul style="list-style-type: none"> • Average Air Temp; Tavg • Vapour Pressure Deficit; VPD • Incoming Shortwave Radiation; srad • Total Precipitation; rain 	~1 km, Monthly , 1982-2022. Gridded climate products based on topographically conditional spatial interpolation of weather stations.	ANUClimate, https://dapds00.nci.org.au/thredds/catalogs/gh70/catalog.html (Hutchison et al., 2014)
Atmospheric CO ₂ concentration	N/A., Monthly , 1982-2022. Extracted from the Cape Grim Baseline Air Pollution Station in Tasmania, Australia. De-seasonalised using a 12-month running mean.	CSIRO Environment and the Australian Bureau of Meteorology (Kennaook / Cape Grim Baseline Air Pollution Station). https://capegrim.csiro.au/
Woody Cover Fraction; WCF	25m, Annual , 1982-2022. A per-pixel estimate of woody cover fraction across Australia. Annual product for 1990-2022. A five-year average from 1990-1995 was used to extend the product back to 1982.	https://dapds00.nci.org.au/thredds/catalog/ub8/au/LandCover/DEA_AL_C/catalog.html (Liao et al., 2020)

140

2.2 Assessment of existing NDVI products

We compared NDVI_{AVHRR} datasets with NDVI_{MCD43A4} for the overlapping period from March 2000 to December 2013. Per-pixel Pearson correlation (r) and coefficient of variation (CV; root mean square error divided by the long-term mean NDVI_{MCD43A4}) describe the agreement between datasets, in addition to comparison of the long-term seasonal cycle. Next, NDVI_{AVHRR} datasets were compared to rolling annual mean 'z-score' standardised anomalies of NDVI_{Landsat} for 1988-2000 to assess how well each product reproduces inter-annual variability in vegetation condition in the pre-MODIS era. Z-score standardised anomalies are calculated as $(x - \mu) / \sigma$ where x is a monthly NDVI observation, μ is the long-term mean NDVI for the given month, and σ is the long-term standard deviation in NDVI for the given month. Differences in spectral sampling between MODIS and Landsat result in differences in mean NDVI so we use Landsat only for validating inter-annual variability in the pre-MODIS era since mean differences in NDVI between sensors are removed by anomalies. We compared NDVI anomalies in NDVI_{Landsat} with NDVI_{MCD43A4} during an overlap period from 2000-2012 to ensure NDVI_{Landsat} could

145

150

Formatted: Subscript

provide a consistent evaluation of interannual variability in the pre-MODIS era and found good agreement between the two products (Fig. A2).

2.3 Calibration and harmonisation

During extensive preliminary testing gradient-boosting decision tree ensembles (GBM), random forest, and generalised additive models were assessed for their ability to calibrate and harmonise $NDVI_{CDR}$ with $NDVI_{MCD43A4}$. The GBM outperformed the other approaches. Two classes of models and datasets were built: one that utilises climate data (hereafter referred to as ‘clim’ models) in the feature set to achieve the best possible agreement between $NDVI_{CDR}$ and $NDVI_{MCD43A4}$. The second excludes climate features (hereafter, ‘noclim’ model) while still achieving satisfactory results. When examining drivers of change, users of these datasets may prefer to use the no-climate model to limit potential circularities in attribution of the drivers of change. During testing, climate variables were identified as useful features for both improving predictions in the heavily forested regions where there was little to no agreement between $NDVI_{MCD43A4}$ and $NDVI_{AVHRR}$, and for capturing interannual variability. The ‘noclim’ models used the following features: solar-zenith-angle (SZEN), time-of-acquisition (TOD), month-of-year, latitude, and $NDVI_{MCD43A4}$ summary percentiles (0.05, 0.5, and 0.95). $NDVI_{MCD43A4}$ summary percentiles were calculated per pixel over the 2000-2022 period. The ‘clim’ models used the same variables, plus incoming solar radiation, rainfall, temperature, and vapour pressure deficit. Fractional anomalies of the climate features are also included, along with cumulative three- and six-month rainfall. Testing revealed the best results were obtained by generating three separate models for areas with high and low woody cover fraction (WCF), and for the desert bioclimatic region (Fig. 1a and Fig. 2a). The long-term mean of WCF was extracted from Liao et al. (2020) and a threshold of $WCF=0.25$ was used to separate regions with a high woody canopy cover. This threshold was chosen as it approximately delineated those regions with the poorest correspondence between $NDVI_{CDR}$ and $NDVI_{MCD43A4}$ (Figure 3e-h).

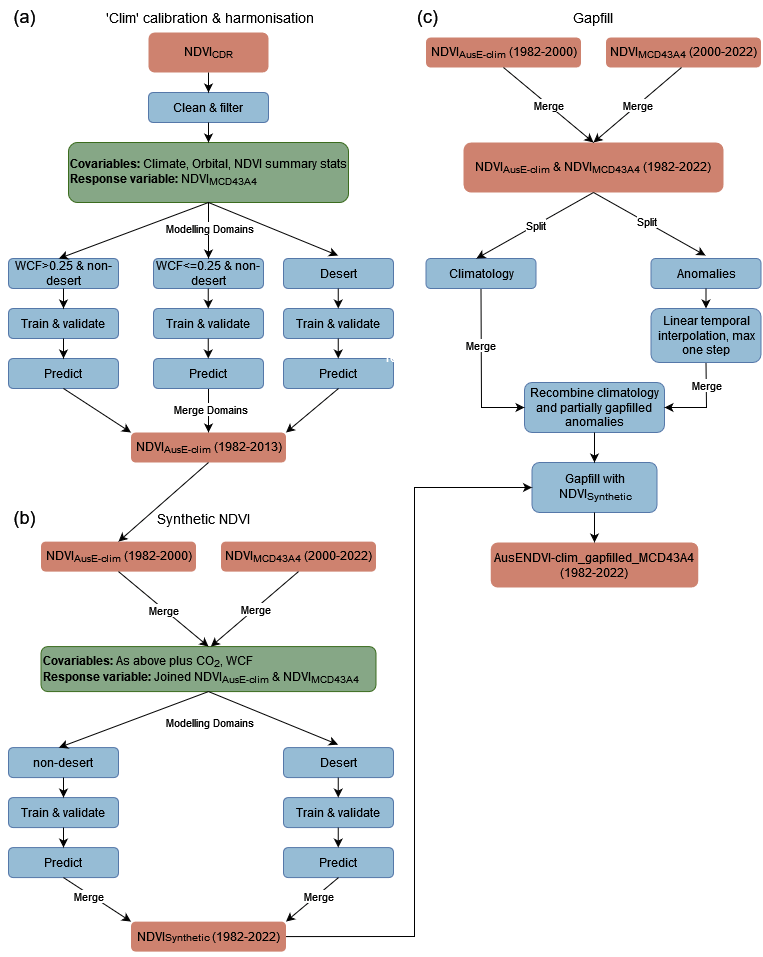


Figure 1: Flowchart describing the calibration and harmonisation methods (a), and the development of a synthetic NDVI (b) for gap filling (c). a) Shows the method for the 'clim' model type, the methods for 'noclim' are the same but climate variables are removed from the covariables and 'noclim' is not gap filled. Red coloured boxes denote datasets, blue boxes denote processing steps, and green boxes describe the response variables and covariables used for modelling.

Owing to the differing volumes of good quality data across the continent (Fig. A1) and the large difference in land area of each bioclimatic region, we implemented a stratified, equalised random sampling approach for the training and validation samples to reduce bias in the sample allocations. In the high and low WCF regions, 30,000 training and testing samples were drawn using an equalised random sampling stratification where a total of 30,000 samples were extracted in equal measure from the five remaining bioclimatic regions after excluding the desert (i.e., 6,000 samples per region). Bioclimatic regions were identical to those defined by Haverd et al. (2013) (Fig. 2+b). In the desert region, samples were drawn using a simple random approach. In all modelling domains, samples were drawn from any point in time across the overlap period, and 5,000 samples were randomly separated as an independent validation set, leaving 25,000 samples for training. The calibration and harmonisation process are summarised in the flow chart of Figure 1a.

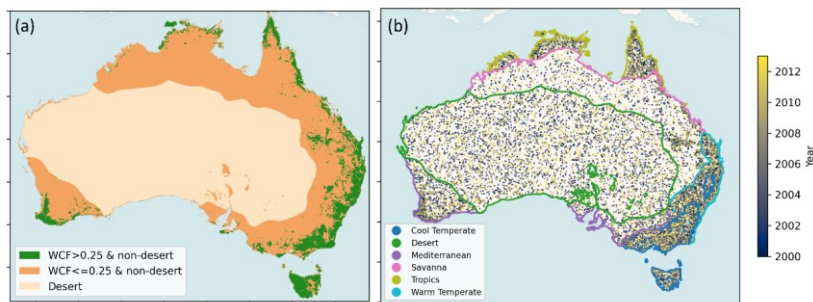


Figure 21: a) Regions delineating the spatial extent of the three modelling domains: desert, low woody cover fraction (WCF) and high WCF. b) The distribution of all independent validation points used to assess the model fits across the three modelling domains in (a); points are coloured by the year they are drawn from. Figure is overlaid with outlines of the six bioclimatic regions used to both stratify training points and for aggregating trends in later analysis.

Cross validation for model hyperparameter optimization was conducted using a nested cross-validation approach with five outer splits and three inner splits (Cawley and Talbot, 2010), the hyperparameter grid search parameters are listed in Table A1. Mean absolute error (MAE), root mean square error (RMSE), and the coefficient of determination (r^2) are reported as indicators of the goodness of fits. To understand which explanatory variables most impacted predictions, feature importance plots

were produced using the Shapley Additive Explanations (SHAP) Python library (Lundberg and Lee, 2017).

2.3 Gap-filling

210 At times there are long gaps in AVHRR data acquisition over Australia. For example, 1994 is entirely missing, and during sensor transition periods the data becomes unreliable for several months before and after the transitions (Tian et al., 2015). Furthermore, owing to the nature of Australia’s prevailing weather systems such as the tropical monsoon, it is not uncommon to have whole geographic regions missing for a given month. This undermines the typical approaches to gap filling that work well when either the
215 temporal gap is short (e.g., temporal interpolation methods using linear or polynomial fits), or the spatial pattern of gaps are quasi-random such as from scattered cloud cover (spatial interpolation methods such as nearest neighbour, kriging etc.) (Bessenbacher et al., 2022; Shen et al., 2015). Gap-filling with a climatology can often mask important interannual variability at key times – such as anomalously high rainfall periods associated with La Niñas when enhanced cloud cover masks large-scale greening events
220 across Australia’s northern tropical savanna. To avoid this we used well established machine learning approaches that have been developed to fill gaps in univariate data (Gerber et al., 2018; Zeng et al., 2014). Here, we develop a two-stage process for gap-filling (summarised in Fig. 1b-c). Firstly, to fill short temporal gaps, the time series is split into a climatology and anomaly series and linear temporal interpolation is applied to the anomalies for a maximum of one time-step (i.e., one month). Longer
225 temporal gaps are replaced with a synthetic NDVI dataset generated using a similar GBM machine learning method as the harmonisation and is described further below.

2.3.1 Synthetic NDVI

Training samples were extracted from $NDVI_{AusE-clim}$ for 1982-2000 and $NDVI_{MCD43A4}$ for 2000-2022, using a similar sampling approach as used for harmonisation only in this instance two models are built, a
230 ‘desert’ model and ‘non-desert’ model. The non-desert model covers the same region as the high and low WCF models previously described (the inclusion of WCF in the features reduces the need to define a low and high WCF modelling region). GBM models were then fit using all the features previously listed for

the ‘clim’ model, plus de-seasonalised CO₂ concentration and annual WCF. Otherwise, the modelling framework was the same as the harmonisation approach (Fig. 1b). The synthetic NDVI datasets (NDVI_{SYN}) are used to gap fill the NDVI_{AusE-clim} record from January 1982 to February 2000. The final gap-filled, calibrated, and harmonised NDVI_{AusE-clim} dataset is joined with NDVI_{MCD43A4}. Only the NDVI_{AusE-clim} dataset is gap filled, the NDVI_{AusE-noclim} dataset is simply joined with the NDVI_{MCD43A4} record. This ensures the ‘noclim’ dataset does not contain any climate information in the reconstructed time series.

240 **2.4 Trends in peak-of-season phenology**

Annual, per-pixel NDVI land surface phenology statistics were extracted using the “xr_phenology” Python function from the “dea-tools” package (Krause et al., 2021). This analysis focused on two metrics, the NDVI value at the peak of the season (vPOS), and the day-of-year the peak occurs (POS). The input time-series was the gap-filled ‘clim’ dataset, and the time-series was first linearly up-sampled from monthly to two-week intervals to increase the temporal resolution of the datasets before the time-series was smoothed using a Savitsky-Golay filter with a window length of 11 and a polynomial order of three. Though we report day-of-year as the unit for POS, the actual POS could have occurred anytime within a given bi-monthly time step, so DOY values should be considered an approximation.

To avoid applying phenology trend analysis on regions that do not experience regular seasonal variation, we created a mask that removes regions identified as ‘non-seasonal’ using the definitions and methods defined by Moore et al. (2016). Broadly, the mask is created using three inputs: the standard deviation in NDVI anomalies, long-term mean NDVI, and the standard deviation in the mean seasonal cycle. These three inputs are used to identify regions that experience either low seasonal variability and low NDVI, or low seasonal variability and high interannual variability, which largely coincide with the desert bioclimatic region.

Per-pixel linear trends in these phenology metrics were extracted using the Theil-Sen robust regression approach, and significance was determined using a Mann Kendall test (significance defined $\alpha = 0.05$). Trends summarised over bioclimatic regions were extracted by first calculating per-pixel robust

regression on the phenology statistics, and then summarising the trends within a bioclimatic region with
260 kernel density estimation (KDE) plots.

3 Results

3.1 Quality of existing datasets.

The quality of the NDVI_{AVHRR} products were compared against NDVI_{MCD43A4} for the overlapping years
2000-2013. All datasets except NDVI_{PKU-consolidated} perform poorly over regions with perennially high
265 vegetation cover including wet coastal and highland forest ecosystems, where correlations between
NDVI_{AVHRR} and NDVI_{MCD43A4} are close to zero in some regions (Fig. 3e-g). NDVI_{CDR} and NDVI_{GIMMS3g}
also poorly represent the desert region with R values are as low as ~0.4 - 0.5. NDVI_{PKU-consolidated} correlates
very well with NDVI_{MCD43A4} over most of the continent, with the exception of western Tasmania (Fig.
3h). Coefficients of variation are also high for the NDVI_{GIMMS3g} and NDVI_{PKU} datasets across much of
270 the continent with average values of 0.33 and 0.18, respectively (Fig. 3b-c).

To demonstrate how the discrepancies over densely vegetated ecosystems would impact, Figure
3j-k presents a zonal timeseries of the woodlands of south-west Western Australia. These woodlands have
been identified as a region of high endemic biodiversity (Myers et al., 2000; Hopper and Gioia, 2004),
are vulnerable to the effects of long-term climate change, and are undergoing long-term shifts in climate
275 (O'donnell et al., 2012; Hughes, 2011; Pitman et al., 2004; Hope et al., 2006). The MODIS-era interannual
variability of these forests are shown through a rolling twelve-month mean timeseries (Fig. 3j) and reveal
that all products capture interannual variability of the MODIS era reasonably well, though the long-term
mean NDVI value varies substantially between products. The mean seasonal cycle, shown in Figure 3k
(calculated from 2001-2013), reveals that the seasonal cycle of the forest ecosystem is very poorly
280 represented in three of the four products, while NDVI_{PKU-consolidated} tracks the overall shape of the seasonal
cycle well, ~~but predicts a longer growing season.~~ Discrepancies in seasonality are further highlighted in
the per-pixel climatological 'month-of-maximum' NDVI plots (Fig. A3). Estimates of even this relatively
straightforward metric of seasonality are impacted by the choice of dataset, with desert, savanna, and
forested regions varying substantially between datasets, sometimes by as much as several months in the

285 case of forested regions in Tasmania and south-east Australia. The Australian-wide seasonal cycles likewise reveal substantial variation between products (Fig. A3g).

To assess the quality of NDVI_{AVHRR} products in the pre-MODIS era, Figure 4a compares the twelve-month rolling mean standardised anomalies of NDVI_{Landsat} in the 1988-2000 period (based on a 1988-2012 climatology) with NDVI_{AVHRR} anomalies. No product accurately tracks NDVI_{Landsat} anomalies across the whole 1988-2000 period. Only the NDVI_{PKU} product captures the amplitude of the La Niña driven positive anomaly of NDVI in 2000 (but recall that NDVI_{PKU} is trained on the NDVI_{Landsat} archive). In Australia, annual rainfall and NDVI anomalies are strongly correlated across the majority of Australia's land mass (Fig. 4c), demonstrating that vegetation growth across the continent is strongly water-limited (Peters et al., 2021; Poulter et al., 2014; Broich et al., 2014). It is therefore our expectation that similarly large negative and positive rainfall anomalies should result in similar NDVI anomalies in the pre-MODIS and MODIS eras. Taking the best of the products identified in the comparison with NDVI_{MCD43A4}, Figure 4b shows the ~~three~~twelve-month rolling mean standardised anomalies of NDVI_{PKU-consolidated} from 1982-2022. In the MODIS era, NDVI_{PKU-consolidated} responds strongly to anomalies in rainfall (background shading shows the continental average standardised rainfall anomalies), while in the pre-MODIS era significant droughts (e.g., 1982-83) and widespread rainfall events (e.g., 2000) produce comparatively little effect in NDVI, suggesting a lack of rainfall-driven variability over Australia in the pre-MODIS era. We develop the statistical relationships between annual mean standardised rainfall and NDVI anomalies, averaged across Australia, for the NDVI_{MCD43A4} and NDVI_{PKU-consolidated} products to quantify their sensitivity to water-supply. Considering the slope of the linear relationship between rainfall and NDVI to be an approximation of the sensitivity of NDVI to water supply, then NDVI_{PKU-consolidated} in the 2000-2022 period displays a similar sensitivity (slope = 1.36, Fig. 4f) and correlation ($r^2=0.56$) as NDVI_{MCD43A4} does in the same period (slope=1.13, $r^2=0.54$, Fig. 4d). Contrast this with NDVI_{PKU-consolidated} in the 1982-2000 period where the apparent sensitivity is approximately half that of the 2000-2022 period (slope=0.65, Fig. 4e). While we may expect some changes in water-supply sensitivity over the decades due to effects such as CO₂

Formatted: Subscript

Formatted: Subscript

Formatted: Superscript

Formatted: Subscript

Formatted: Superscript

Formatted: Subscript

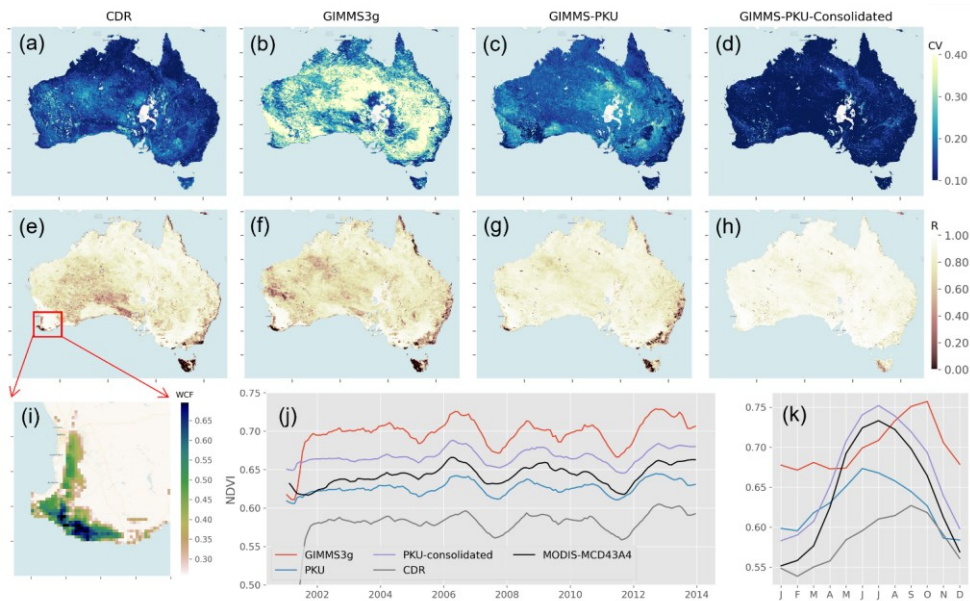


Figure 3: Comparisons between $NDVI_{MCD43A4}$ and four versions of $NDVI_{AVHRR}$. a-d) The coefficient of variation (CV) between $NDVI_{MCD43A4}$ and $NDVI_{AVHRR}$ where RMSE is divided by the 2001-2013 mean of $NDVI_{MCD43A4}$. e-h) Pearson correlation (r) between $NDVI_{MCD43A4}$ and $NDVI_{AVHRR}$. i) Woody cover fraction (WCF) of the forests in south-west Western Australia indicating the location of the zonal time-series of (j) and (k). j) Twelve-month rolling mean NDVI timeseries of the forests of south-west Western Australia. k) Mean seasonal cycle of the forests of south-west Western Australia calculated over the 2001-2013 period.

fertilisation (Donohue et al., 2013; Ukkola et al., 2016), a doubling of water-supply sensitivity is highly unlikely. Thus, we argue that no current $NDVI_{AVHRR}$ product currently satisfies our criteria of a product that both agrees well with $NDVI_{MCD43A4}$ while also producing satisfactory results in the pre-MODIS era.

3.2 Calibration and harmonisation performance

Independent validation statistics for all six model varieties ('clim' and 'noclim'; desert, high and low WCF) reveal a high degree of agreement in all model types with $r^2 \geq 0.91$ for the 'clim' models, RMSE ≤ 0.039 , and MAE ≤ 0.028 (Fig. 5a-c). The 'clim' model types tended to have errors ~15 % smaller

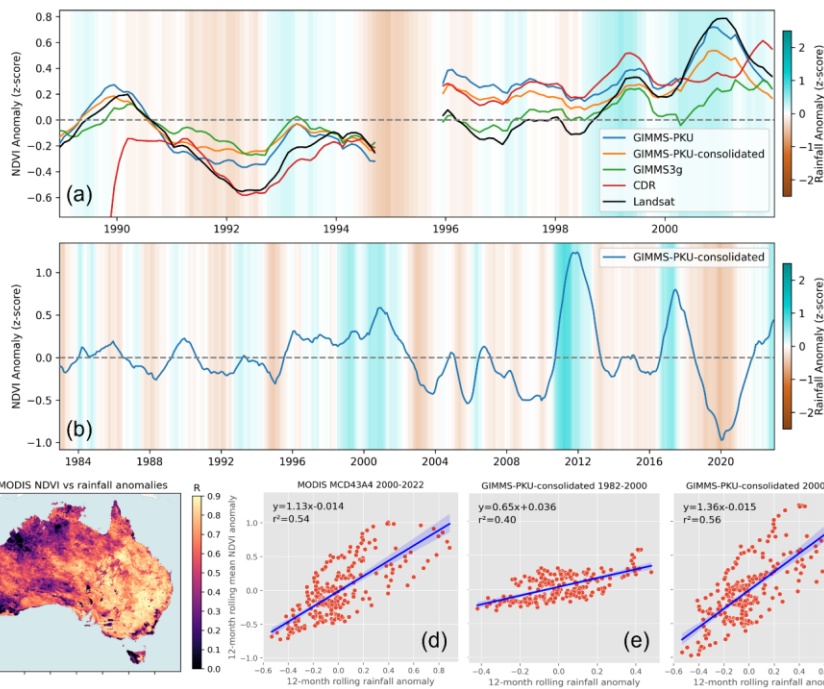


Figure 4: a) Twelve-month rolling mean standardised anomalies of Landsat, CDR, GIMMS3g, GIMMS-PKU, and GIMMS-PKU-consolidated NDVI, based on a common 1988-2012 climatology. Background shading represents twelve-month rolling mean standardised rainfall anomalies. All datasets, besides rainfall, have matching data gaps. b) Twelve-month rolling mean standardised anomalies of the $NDVI_{PKU-consolidated}$ product (1982-2022 climatology). c) Pearson correlations between annual $NDVI_{MCD43A4}$ anomalies and annual rainfall anomalies, shown here to demonstrate the strongly water limited nature of Australia's vegetation. d-f) Relationships between twelve-month standardised rainfall and NDVI anomalies averaged across Australia for different periods and different products. In (d) $NDVI_{MCD43A4}$ and rainfall anomalies have been calculated against a 2000-2022 baseline. In (e-f) rainfall and $NDVI_{PKU-consolidated}$ anomalies have been calculated against a 1982-2022 baseline. The relationships $y=mx+c$ denotes the linear regression slope between rainfall and NDVI anomalies where y is NDVI anomalies, x is rainfall anomalies, and m is the slope coefficient. The slope coefficient can be considered an approximation of the sensitivity of NDVI to anomalous water supply aggregated over the continent.

than their 'noclim' counterparts (Fig. 5d-f). SHAP feature importance plots indicate $NDVI_{CDR}$ as the most important variable (Figure A3), but in the high WCF regions the relative importance of $NDVI_{CDR}$ diminished and $NDVI_{MCD43A4}$ summary statistics, solar radiation, and cumulative rainfall substantially

impacting predictions (Figure A4b,c). ~~Orbital parameters (SZEN, TOD) tended to have little effect on predictions regardless of model type.~~

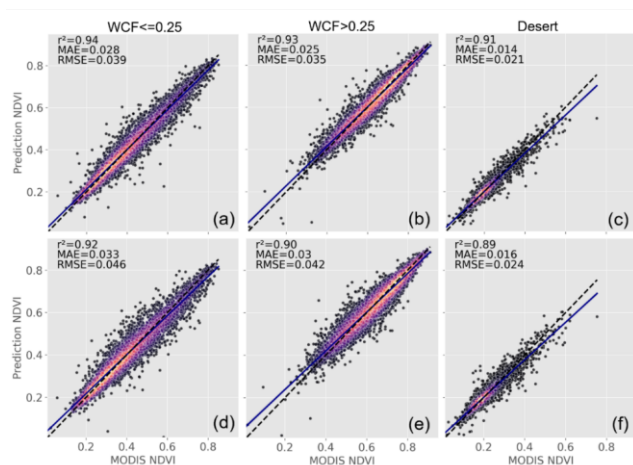
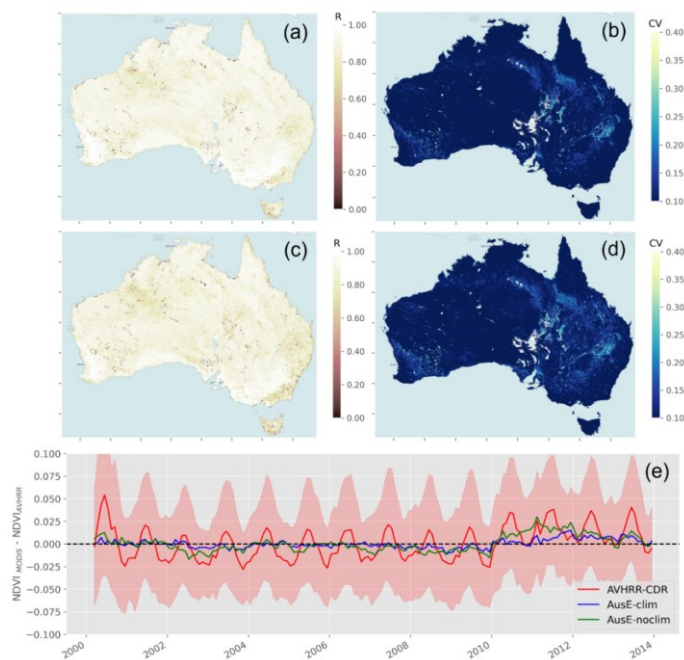


Figure 5: Validation scatter plots for the calibration and harmonisation between $NDVI_{CDR}$ and $NDVI_{MCD43A4}$. (a-c) show the results for the 'clim' model. (d-f) shows the same but for the 'noclim' model type.

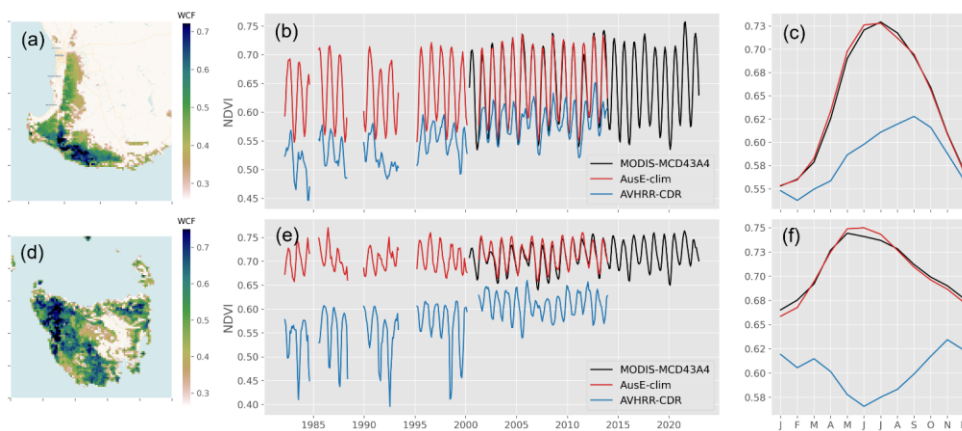
Per pixel agreements between $NDVI_{AusE}$ and $NDVI_{MCD43A4}$ for both the 'clim' and 'noclim' model types reveal a very high degree of correlation across the continent (note that pixels with a long-term average $NDVI \leq 0.11$ are masked for this analysis). Correlations between $NDVI_{MCD43A4}$ and $NDVI_{AusE}$ in Australia's forested ecosystems have been greatly improved, averaging Pearson R = 0.8590 (Fig. 6a) in the 'clim' model (average Pearson R in the CDR = ~~product is 0.4858~~). Areas of lower correlation persist in places that experience ephemeral or periodic water inundation such as mangroves and inland lake systems. Relative error has been reduced universally across the continent, with a continental average CV of <10 % (Fig. 6b). Areas of greatest relative error occur in the channel country in Australia's arid interior, and the irrigated regions of the northern Murray Darling Basin. The 'noclim' model performs similarly, though correlations and relative error are universally worse than the 'clim' model (Fig. 6c-d). Residual NDVI values after subtracting $NDVI_{AVHRR}$ from $NDVI_{MCD43A4}$ before and after the calibration and harmonisation show the GBM model has entirely removed the residual seasonal signal present in the CDR

360 product, resulting in residuals that closely track the zero line. Some small bias remains in the 2011-2012
 period (particularly for the 'noclim' model) when anomalously large rainfall related to a major La Nina
 event resulted in anomalous greening in the savanna and desert biomes. This is further illustrated in
 Figure A5 where NDVI timeseries before and after the adjustment have been summarised over six
 bioclimatic regions (extents in Fig. 2b). Differences in the Australia-wide time-series between
 365 $NDVI_{MCD43A4}$ and $NDVI_{AusE}$ are largely attributable to $NDVI_{AusE}$ underestimating peak NDVI during
 2011-2012 in the desert and savanna biomes (Fig. A5f-g).



370 **Figure 6: Results of the calibration and harmonization between $NDVI_{CDR}$ and $NDVI_{MCD43A4}$. a) shows the per pixel Pearson correlation, between $NDVI_{MCD43A4}$ and 'clim' $NDVI_{AusE}$. b) shows the same as (a) but for the coefficient of variation. c-d) the same as (a-b) but for the 'noclim' model type. e) The residual NDVI value when subtracting $NDVI_{AVHRR}$ from $NDVI_{MCD43A4}$ before and after the calibration and harmonization. Residuals are calculated per pixel and then averaged over Australia. Shading indicates the standard deviation in residuals across the continent for the $NDVI_{CDR}$ product.**

Improvements in the alignment between $NDVI_{CDR}$ and $NDVI_{MCD43A4}$ from this regional calibration and harmonisation are further demonstrated in Figure 7 where timeseries are summarised over two challenging forest ecosystems in southwest Western Australia and Tasmania. Mean seasonal cycles between the two NDVI datasets are now in very close agreement (Fig. 7c, f) and the $NDVI_{AusE-clim}$ time-series from 1982-2000 can effectively integrate with the $NDVI_{MCD43A4}$ time-series without introducing major discontinuities (Fig. 7b, e). Note also that the GBM calibration has ameliorated the strong increasing trend in $NDVI_{CDR}$ from 1982-2000 (Fig. 7b, e) that is almost certainly due to artificial step changes between sensor transitions and poor calibration over these regions. In the appendix, we replot Figure 7d-f with the inclusion of $NDVI_{GIMMS3g}$ to demonstrate that the trend in $NDVI_{CDR}$ is an artefact of the CDR product (Fig. A6).



385 **Figure 7:** Results before and after the calibration and harmonisation of $NDVI_{CDR}$ for two example high woody canopy cover regions previously identified as having the worst agreement with $NDVI_{MCD43A4}$. b-c) Three-month rolling mean 1982-2022 NDVI time series, and the mean seasonal cycle (averaged over the 2001-2013 period), respectively, for the forests of south-west Western Australia. e-f) Same as (b-c) but for Tasmanian forests. Time series are the spatial average of the regions to their left.

3.2 Gap-filling with Synthetic NDVI

390 The $NDVI_{SYN}$ dataset record agrees exceptionally well with the joined $NDVI_{AusE-clim}$ and $NDVI_{MCD43A4}$ series when aggregated across Australia (Fig. 8e). The time series of Figure 8e is further disaggregated

Formatted: Subscript

Formatted: Subscript

Formatted: Subscript

395 into high and low WCF regions (as per Figure 2a) in Figure A7 and reveals that in densely wooded regions synthetic NDVI tends to underestimate peak seasonal growth, but otherwise captures seasonal timings and inter-annual variability (Fig. A7b). In the low WCF regions (Fig. A7a), synthetic NDVI closely
400 matches observations. At the pixel level, the long-term mean NDVI of both datasets is virtually identical (Fig. 8a-b). Per-pixel Pearson correlation averages 0.85 across the continent (Fig. 8d). Areas of poorer correlation occur in western Tasmania, the highlands forests of south-east Australia – all areas that experience seasonal snow fall – and regions of either anthropogenic water application (irrigation) or ephemeral, delayed water inundation (inland rivers in the arid interior). Mean relative error was also low, averaging 11 %, but with hotspots of greater error again occurring in the regions where water inundation is not dependent on direct rainfall (Fig. 8c)– The results before and after gap filling NDVI_{AusE-clim} are presented in Figure 8f. As missing data tends to be in the higher NDVI regions (wetter, cloudier, forested regions), gap filling has the tendency of increasing NDVI when averaged over the continent.

405 We present validation scatter plots and feature importance plots for the desert and non-desert GBM models in the appendix (Fig. A8). In the non-desert region, three-month cumulative rainfall and VPD are the key climate drivers of predictions, while in the desert region, six-month cumulative rainfall, VPD, and incoming solar radiation are the key climate drivers.

Formatted: Subscript

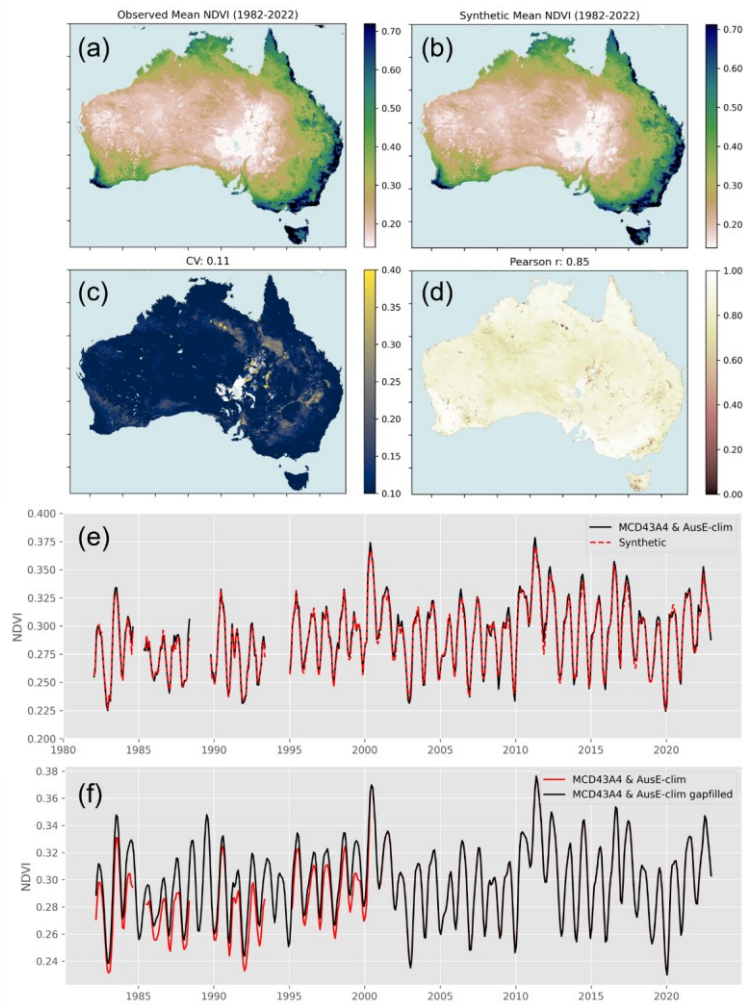


Figure 8: Evaluation of the synthetic NDVI built to gap-fill the $NDVI_{AusE-clim}$ record a-b) show the observed and synthetic long-term mean NDVI, respectively. c) per pixel coefficient of variation (CV) between observed NDVI and synthetic NDVI. d) Same as (c) but Pearson correlation. e) Continentally averaged observed and synthetic NDVI timeseries, where data gaps have been matched. **f) The results of gap filling the merged $NDVI_{AusE-clim}$ and $NDVI_{MCD43A4}$ time series.**

410

415

3.3 Assessing interannual variability~~Comparison with Landsat and MODIS NDVI annual time series~~

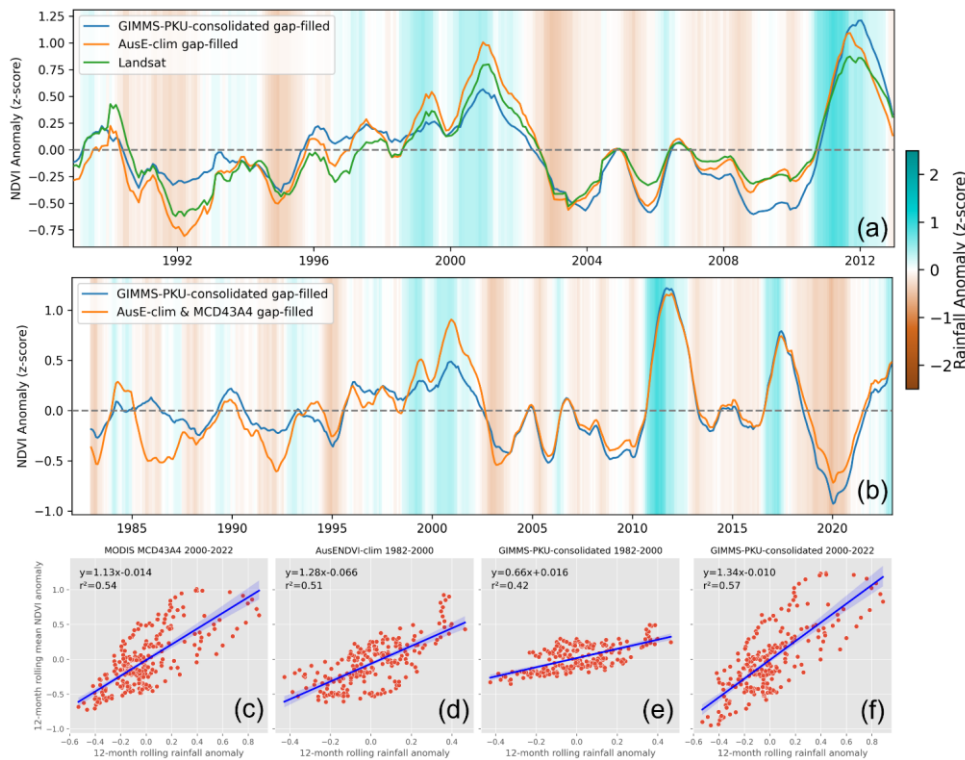
Comparing the calibrated, harmonised, and gap-filled $\text{NDVI}_{\text{AusE-clim}}$ dataset with rolling annual mean $\text{NDVI}_{\text{Landsat}}$ anomalies reveals a good level of agreement in both the timing and magnitude of inter-annual variability throughout the 1988-2012 period (Fig. 9a). $\text{NDVI}_{\text{PKU-consolidated}}$ is also shown for comparison and gaps in the $\text{NDVI}_{\text{PKU-consolidated}}$ dataset have been filled using the same synthetic data and procedure as $\text{NDVI}_{\text{AusE-clim}}$ to facilitate a more straightforward comparison and continuous time-series. $\text{NDVI}_{\text{AusE-clim}}$ consistently outperforms $\text{NDVI}_{\text{PKU-consolidated}}$ throughout the Landsat series. IAV in $\text{NDVI}_{\text{AusE-clim}}$ is further assessed in Figure 9b where the full time series (1982-2022, joined with $\text{NDVI}_{\text{MCD43A4}}$) and $\text{NDVI}_{\text{PKU-consolidated}}$ are plotted together as rolling annual mean standardised anomalies against the same 1982-2022 climatology. $\text{NDVI}_{\text{AusE-clim}}$ clearly displays greater IAV in the pre-MODIS era. We repeat the same analysis as in Figure 3d-f but this time including $\text{NDVI}_{\text{AusE-clim}}$. The NDVI-rainfall relationships show that $\text{NDVI}_{\text{AusE-clim}}$ reports a similar water-supply sensitivity and correlation in the 1982-2000 period (slope=1.28, $r^2=0.51$, Fig. 8d) as MODIS does in 2000-2022 period (slope=1.13, $r^2=0.54$, Fig. 9c). Again, while we may expect some changes in water-supply sensitivity over the decades due to effects such as CO_2 fertilisation, water supply sensitivity ought to remain relatively stationary, and we take the correspondence between $\text{NDVI}_{\text{MCD43A4}}$ sensitivity and $\text{NDVI}_{\text{AusE-clim}}$ sensitivity as an indication that $\text{NDVI}_{\text{AusE-clim}}$ is responding realistically to interannual variations in rainfall.

A comparison with $\text{NDVI}_{\text{MCD43A4}}$ is shown in Figure 8b where all three time series are plotted as a simple rolling annual mean. $\text{NDVI}_{\text{AusE-clim}}$ aligns well with $\text{NDVI}_{\text{MCD43A4}}$ at the annual timescale and records greater rainfall driven inter-annual variability in the pre-MODIS era. The historic 1982-2000 archive can clearly join with the $\text{NDVI}_{\text{MCD43A4}}$ series without introducing major discontinuities.

Formatted: Not Superscript/ Subscript

Formatted: Subscript

Formatted: Subscript



440 **Figure 9:** a) Twelve-month rolling mean standardised NDVI anomalies of the gap-filled $NDVI_{AusE-clim}$ plotted alongside Landsat anomalies and $NDVI_{PKU-consolidated}$ anomalies. Gaps in the $NDVI_{PKU-consolidated}$ dataset have been filled using the same synthetic data and procedure as $NDVI_{AusE-clim}$. All datasets are matched to Landsat data gaps. b) Twelve-month rolling mean standardised anomalies of the $NDVI_{PKU-consolidated}$ (gap-filled in the same manner as (a)), and $NDVI_{AusE-clim}$ joined with $NDVI_{MCD43A4}$ (1982-2022 climatology). c-f) Relationships between twelve-month standardised rainfall and NDVI anomalies averaged across Australia for different periods and different products. Rainfall, $NDVI_{AusE-clim}$ and $NDVI_{PKU-consolidated}$ anomalies have been calculated against a 1982-2022 baseline. $NDVI_{MCD43A4}$ anomalies have been calculated against a 2000-2022 baseline. The slope coefficient can be considered an approximation of the sensitivity of NDVI to anomalous water supply aggregated over the continent. Note that the slope and intercepts for GIMMS-PKU-consolidated are slightly different to Figure 3 owing to gap filling.

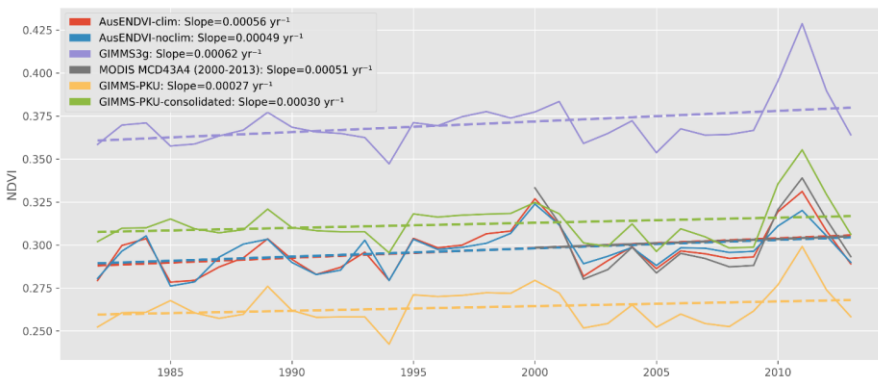
Formatted: Font: 9 pt, Bold, Subscript

Formatted: Font: 9 pt, Bold, Subscript

Formatted: Font: 9 pt, Bold, Subscript

450 **3.4 Annual average trends**

We also evaluated the annual-average NDVI trends across Australia to assess the performance of AusENDVI in reproducing greening trends observed in other products. Trends were calculated over the overlapping period of 1982-2013 using ordinary least squares regression after aggregating NDVI data to annual means. AusENDVI closely reproduces the observable trends in NDVI_{GIMMS3g} (coefficients: AusENDVI-clim=0.00056 NDVI yr⁻¹, AusENDVI-noclim=0.00049 NDVI yr⁻¹, GIMMS3g=0.00062 NDVI yr⁻¹; Fig. 10). Trends in NDVI_{MCD43A4} over the shorter interval from 2000-2013 displayed a similar slope to AusENDVI and GIMMS3g (0.00051 NDVI yr⁻¹). Trends in the two GIMMS-PKU products are approximately half those of the other products.



460 **Figure 10: Annual average NDVI trends summarised over Australia for the overlapping period of 1982-2013. All data gaps have been matched between datasets and datasets have been reprojected to match the resolution of GIMMS3g. Note that AusENDVI-clim and noclim have both had data gaps filled to facilitate better annual averaging (i.e., so all years have values). Trend lines have been fitted using ordinary least-squares regression and coefficients are expressed in terms of NDVI per year.**

465 **3.5 Trends in peak-of-season phenology**

Per-pixel trends in vPOS, POS and the 40-year median values for these statistics are shown in Figure 11. Trends in vPOS are almost universally positive across the continent (hatching indicates a significant trend), with the exceptions of inland northern Murray-Darling Basin, the eastern periphery of the wheat

Formatted: Font: 12 pt

Formatted: Font: 12 pt

Formatted: Font: 12 pt

Formatted: Font: 12 pt

Formatted: Font: 12 pt, Subscript

Formatted: Font: 12 pt

Formatted: Font: 12 pt

Formatted: Font: 12 pt

Formatted: Font: 12 pt, Superscript

Formatted: Font: 12 pt

Formatted: Font: 12 pt

Formatted: Font: 12 pt

Formatted: Font: 12 pt, Superscript

Formatted: Font: 12 pt

Formatted: Subscript

Formatted: Superscript

Formatted: Font: 12 pt

Formatted: Font: 12 pt

Formatted: Centered

Formatted: Caption

Formatted: Font: 9 pt

Formatted: Font: 10 pt

Formatted: Justified

470 belt in Western Australia, and the region north of Adelaide (Fig. 11b). Positive trends observed in the
major agricultural region of the Murray-Darling Basin and the northern half of the West Australian wheat
belt and are non-significant. Distributions of trends in vPOS, stratified by bioclimatic region, reveal the
highest median trends are recorded in the tropics and savanna regions at 0.0013 and 0.0014 NDVI yr⁻¹,
respectively (Fig. A9a-e). The Mediterranean region has the lowest median trend at 0.0009 NDVI yr⁻¹.

475 Trends in the day-of-year that peak NDVI occurs (POS) are negative across much of the continent,
suggesting there is a general tendency for NDVI to peak earlier in the year across Australia. Significant
negative trends occur in the agricultural zones of the Mediterranean bioclimatic region, the greater
western woodlands that border the eastern margin of the WA wheatbelt, the western half of the Nullabor
plain, parts of the Riverina agricultural region of south-western New South Wales and extending into
480 Victoria, and western parts of the northern tropical savanna. These significant negative trends are reflected
in the POS trend distributions in Figure A9f-j where the median trend in the warm temperate and
Mediterranean regions are highest at 3.4 and 2.3 days per decade, respectively. Significant positive trends
(peak NDVI occurring later in the year) are observed in tropical northern Queensland and western
Tasmania and can be as high as 5-10 days per decade.

485

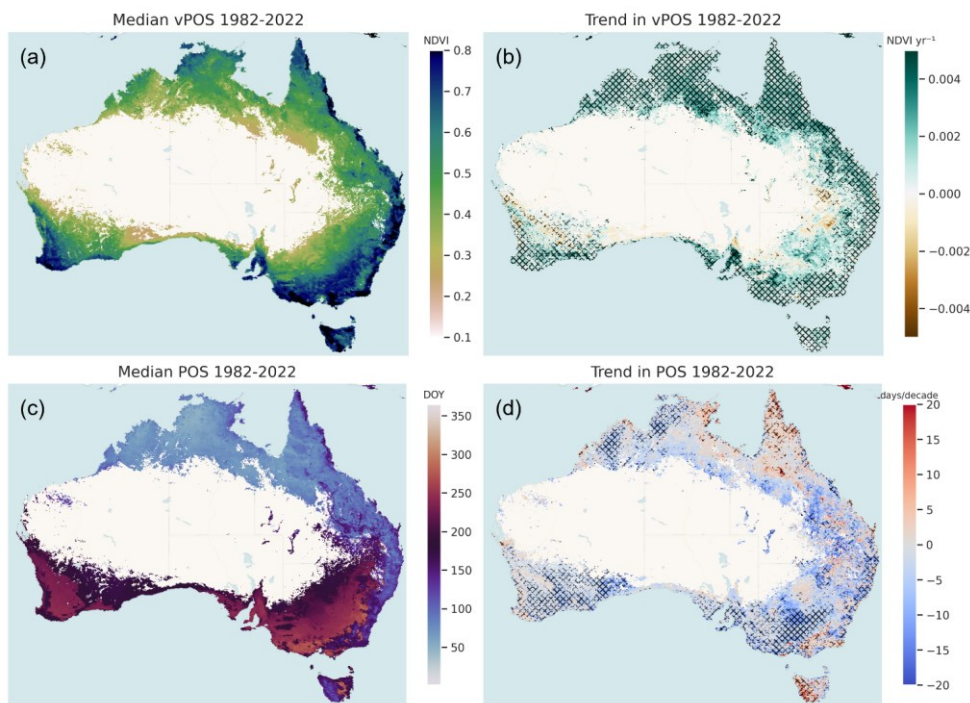


Figure 11: a) The median annual peak NDVI value (vPOS) from 1982-2022. b) Theil-Sen robust regression trends in vPOS. c) Median day-of-year that peak NDVI occurs (POS), 1982-2022. d) Theil-Sen robust regression trends in POS. Hatching on trend plots indicates significance at alpha=0.05 using a Man-Kendall test. All plots are derived from the gap-filled 'clim' NDVI_{AUSE} dataset. Non-seasonal areas have been masked using the method described in section 2.4.

490

4 Discussion

4.1 Limitations of existing global products and improvements by AusENDVI

We expected to identify differences between NDVI_{AVHRR} and NDVI_{MCD43A4} given differences in the spectral sampling between sensors, datasets given their different pre-processing and atmospheric corrections methods, different spatial resolutions, and differing and temporal compositing techniques. Likewise, comparatively lower correlations in the densely vegetated regions were also expected due to

495

Formatted: Heading 2

Formatted: Subscript

the total variance in evergreen forests being smaller than for seasonal vegetation (grassland, croplands), and therefore, assuming a similar unexplained variance (noise), correlations should necessarily be weaker. Nonetheless, we were surprised by the fairly large inconsistencies between NDVI_{GIMMS3g}, NDVI_{CDR}, and NDVI_{GIMMS-PKU} by the poor performance of global NDVI_{AVHRR} products in representing the seasonal dynamics of Australia's densely vegetated regions (e.g. Fig. 3k). Why this is the case deserves a greater focus of study than we devote here but is likely related to some combination of the presence/absence of BRDF and water-vapour corrections, varying contamination by clouds, and any gap-filling procedures applied. Regardless of the reasons why, the intercomparison between NDVI_{AVHRR} products highlights that global datasets, while often performing adequately when statistics are aggregated at the global or continental scale, can mask disparities that are important at the regional to local scale (Meyer and Pebesma, 2022). We advocate closely examining regional and local contexts to assess how suitable a given NDVI dataset is for a particular use case. For example, in Australia seasonal cycles in NDVI_{CDR} are highly suspect and thus should not be relied upon for phenology studies. However, NDVI_{CDR} has a comparatively low relative error when compared with NDVI_{MCD43A4-MODIS} and displays reasonable inter-annual variability so would likely be more suited to long-term studies of agricultural drought frequency or the impacts of CO₂ fertilisation on maximum canopy cover (assuming sensor transitions are filtered). In Australia, the best use of NDVI_{PKU-consolidated} is likely the reverse, its representation of seasonal cycles comports well with NDVI_{MCD43A4} is good, while IAV is subdued in the pre-MODIS era which could lead to incorrect conclusions regarding shifting sensitivities to water supply in Australia's water-limited ecosystems. In general, we urge caution in using existing global NDVI_{AVHRR} products for studying vegetation trends and seasonality in Australia. AusENDVI shows significant improvement over existing global datasets in this respect. The improved correspondence in seasonal cycles between AusENDVI and NDVI_{MCD43A4} provides evidence that AusENDVI is more suitable for exploring longer-term changes to Australia's vegetation phenology. Moreover, the addition of climate features to the calibration and harmonisation also appears to have improved the representation of long-term interannual variability and trends in annual average NDVI, thus AusENDVI-clim should likewise offer a better basis for studying the shifting frequency of extreme climate events and their impact on the terrestrial biosphere.

Formatted: Subscript

4.2 Synthetic NDVI

The creation of a synthetic NDVI using only climate, CO₂ concentration, and woody cover fraction as predictors revealed a high degree of predictability in NDVI over much of Australia. Regions of lower predictability were located where water supply is either from elsewhere or delayed (ephemeral inland rivers) ~~or~~ or from irrigation. In the absence of features that could describe water supply without rainfall, NDVI patterns in these zones will continue to be difficult to estimate if direct satellite observations are unavailable. Notwithstanding some spatial variability in per-pixel predictability, in general the high degree of agreement between observed and synthetic NDVI presents the prospect of extending the synthetic NDVI further back in time through the observational climate record, which in Australia is reliable throughout much of the 20th century. In land surface models, a dynamic phenology algorithm is an important sub-model which influences the overall carbon cycle, evapotranspiration, and energy balance of the model (Chen, 2022). The long-term record of synthetic NDVI developed here could, therefore, prove useful for validating the development of process-based phenology models for Australia's diverse range of vegetation and climate. Or, with empirically validated NDVI-LAI relationships, AusENDVI could be used as a phenology forcing during the pre-satellite era for the many LSMs that do not dynamically simulate LAI.

4.3 Sources of uncertainty and future work

There are several sources of uncertainty in AusENDVI. Firstly, the climate and landscape features used are subject to their own uncertainties which will undoubtedly propagate into both the calibration and harmonisation, as well as the gap-filling with synthetic NDVI. For example, rainfall station observations in the arid interior of Australia are relatively sparse so errors in the spatial interpolation of rainfall are highly likely. Uncertainties in the NDVI_{CDR} product are also likely to be transmitted to our dataset. Future work may include a greater treatment of uncertainty through ensemble modelling where climate features (e.g., different rainfall and solar radiation datasets), and model types used for fitting are iterated to generate an uncertainty envelope. We also aim to assess how well NDVI from the Visible Infrared Imaging Radiometer Suite (VIIRS) agrees with NDVI_{AusE} and NDVI_{MCD43A4} over Australia. Should there be a substantial discrepancy, the methods described here could be applied to VIIRS to create an ongoing,

Formatted: Font: 12 pt

Formatted: Font: 12 pt

Formatted: Heading 2, Indent: First line: 0 cm

Formatted: Heading 2, Indent: First line: 0 cm

updated NDVI dataset for Australia than can continue to form the foundation for continental-scale studies of terrestrial ecosystem change. Irrespective, we argue our AusENDVI estimates are based on the best available data, while the gradient boosting models have gone through extensive cross-validation. Therefore, we contend that the resulting trends should be more accurate than any alternative NDVI dataset.

4.4 Trends in peak of season phenology

We identified advances in the timing of POS across much of Australia's land mass (though not all). Over the Mediterranean, warm temperate, and cool temperate bioclimatic regions the median peak phenology trends were -2 to -3 days/decade. Advances in plant maturity in the southern hemisphere from field data are also reported by Chambers et al. (2013) where the mean rate of change in plant maturity was 14 days/decade, mostly from temperate regions (63 % of their data are from grape-vines). This rate of change is comparable to the per-pixel rates of change in POS that are seen in parts of the Mediterranean and warm temperate regions where it is not uncommon to see negative trends ranging from 10-15 days/decade (Fig. 11d). However, the magnitude of a trend is influenced by the length of the time series so comparisons with variable length field data is difficult and shorter records are more likely to report a larger rate (Chambers et al., 2013). Advances in the timing of POS could be due to a combination of climate drivers. In the northern hemisphere, warming has led to earlier peak greening (Huang et al., 2023; Liu et al., 2021; Park et al., 2019). Warming can accelerate metabolism, so where water is non-limiting, leaf development can be faster. However, temperature increases also increase vapour pressure deficits which decrease water-use efficiency and can reduce plant productivity, though this effect may be compensated for by enhanced CO₂ (Rifai et al., 2022; Dusenget al., 2019). Changes in the timing of peak rainfall may also contribute to shifts in the timing of peak NDVI. The timing of peak climatological rainfall has shifted since 1960 (Fig. A10a-c), and there is some coincidence between trends in POS and shifts in rainfall POS (e.g., advancement around Adelaide). The goal of this study is not to draw conclusions on the likely drivers of seasonality change in Australia, but to argue that our dataset provides a more reliable means for tackling these questions. Future work will delve into a greater suite of phenology metrics (e.g., start-

Formatted: Heading 2, Indent: First line: 0 cm

of-season, end-of-season, growing season length (Xie et al., 2023)), and explore the drivers of phenological change.

580 The pervasive positive trends in vPOS are consistent with results elsewhere and are likely due to the impacts of CO₂ fertilisation, which allows a given amount of precipitation to sustain a greater maximum level of plant production over time (Donohue et al., 2009; Donohue et al., 2013; Rifai et al., 2022; Ukkola et al., 2016). Increases in the magnitude of Austral spring and summer rainfall in northern Australia are also likely to have contributed to the widespread increase in vPOS in tropical Australia
585 (Figure A10d). It is also likely that improving agricultural practices has increased maximum NDVI in the rain-fed cropping regions, especially in South Australia and Victoria where positive vPOS trends are significant. Trends in maximum NDVI in the WA wheatbelt are also positive, but contrast with the fact that WA has seen a widespread autumn drying trend (Fig. A10d). We speculate that agricultural innovation here has counteracted a drying trend that would otherwise have reduced foliage cover.

590 **5 Data and Code Availability**

AusENDVI is openly available at <https://doi.org/10.5281/zenodo.10802704> (Burton, 2024) and consists of several datasets. Each dataset has a description in the attributes of the NetCDF file that defines its provenance. A short description of each dataset is provided below as an additional reference. All datasets are in "EPSG:4326" projection, have a spatial resolution of 0.05°, and monthly temporal resolution. A
595 Jupyter notebook is also provided at the above link demonstrating how to load, plot, mask, reproject, and gap-fill AusENDVI datasets.

- *AusENDVI-clim_1982_2013*. Calibrated and harmonised NOAA's Climate Data Record AVHRR NDVI data from January 1982 to December 2013. This version of the dataset used climate data in
600 the calibration and harmonisation process. The dataset has not been gap filled, and extra data has been filtered/removed beyond the typical QA filtering using methods described in this publication.
- *AusENDVI-noclim_1982_2013*. Calibrated and harmonised NOAA's Climate Data Record AVHRR NDVI data from January 1982 to December 2013. This version of the dataset did not use

605 climate data in the calibration and harmonisation process. The dataset has not been gap filled, and extra data has been filtered/removed beyond the typical QA filtering using methods described in this publication.

- *AusENDVI-synthetic_1982_2022*. This dataset consists of synthetic NDVI data that was built by training a model on the joined ‘AusENDVI-clim’ and ‘MODIS-MCD43A4 NDVI’ timeseries using climate, woody-cover-fraction, and atmospheric CO₂ as predictors.
- 610 • *AusENDVI-clim_gapfilled_MCD43A4_1982_2022*. This dataset consists of calibrated and harmonised NOAA's Climate Data Record AVHRR NDVI data from January 1982 to February 2000, joined with MODIS-MCD43A4 NDVI data from March 2000 to December 2022. This version of the dataset used climate data in the calibration and harmonisation process. The dataset has been gap filled using AusENDVI-synthetic,
- 615 • *AusENDVI-noclim_MCD43A4_1982_2022*. This dataset consists of calibrated and harmonised NOAA's Climate Data Record AVHRR NDVI data from January 1982 to February 2000, and MODIS-MCD43A4 NDVI data from Mar. 2000 to Dec. 2022. This version of the dataset did not use climate data in the calibration and harmonisation process. The dataset has not been gap filled.

620 The code to conduct all analysis described here is available on the open-source repository: <https://github.com/cbur24/AusENDVI>

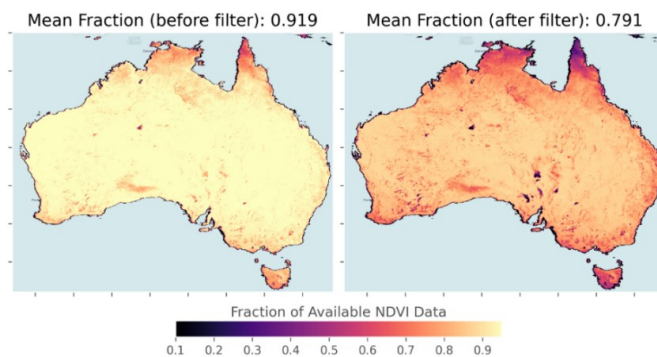
6 Conclusion

625 We calibrated and harmonised NDVI_{CDR} to NDVI_{MCD43A4} for Australia using a well cross-validated gradient-boosting ensemble decision tree method. We developed two versions of the datasets, one that utilises climate data in the feature set to achieve the best possible agreement between NDVI_{CDR} and NDVI_{MCD43A4} (‘AusENDVI-clim’); and a second dataset that does not rely on climate data (‘AusENDVI-noclim’). The resulting datasets have a spatial resolution of 0.05° and extend from 1982-2013 with a monthly time step. We also provide a complete 41-year long dataset where gap filled AusENDVI-clim from January 1982 to February 2000 is seamlessly joined with NDVI_{MCD43A4} from March 2000 to

Formatted: Font: (Default) +Body (Times New Roman)

630 December 2022. The advantages of AusENDVI are that: 1) It closely reproduces the NDVI_{MCD43A4} record in terms of seasonality, interannual variability, and trends in annual-average NDVI; 2) It reproduces annual anomalies in the Landsat NDVI record in the pre-MODIS era (back to 1988), and shows realistic rainfall-driven interannual variability back to 1982; 3) We developed a reliable method for gap filling the AusENDVI record by creating a synthetic NDVI dataset using only climate, CO₂ concentration, and
635 woody cover fraction as predictors. The resulting dataset showed excellent agreement with the observations, providing confidence in its use for gap filling. 4) AusENDVI has a higher spatial resolution than any of the GIMMS-based datasets and is built using inputs that apply the full suite of atmospheric and BRDF corrections; and 5) The methods and code for its development are entirely open-source. No other existing product can lay claim to all these attributes which is why we argue AusENDVI is an
640 important addition to the suite of NDVI products available. We contend it is highly suitable for studying the impact of global environmental change on Australia's terrestrial vegetation.

Appendix



645 **Figure A1: Available fractions of data before and after additional filtering of NDVI_{CDR} data. A value of one means all monthly time-steps between 1982-2013 are preserved.**

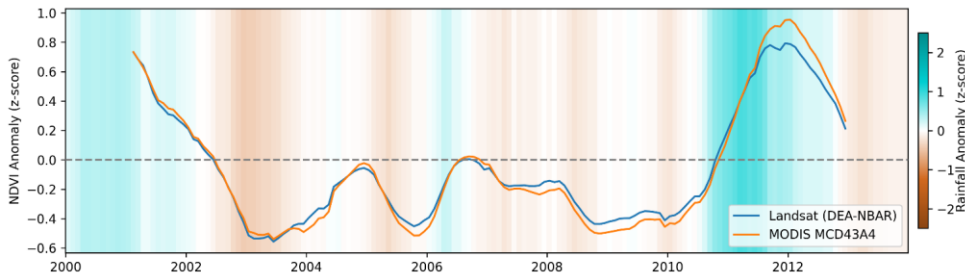


Figure A2: Standardised anomalies of the overlapping period between MODIS MCD43A4 NDVI and DEA's Landsat NDVI derived from the common baseline period of 2000-2012. Rainfall anomalies are derived from a longer baseline of 1982-2022.

Formatted: Caption

Table A1. The hyperparameter grids used during model optimization of the harmonisation model and the synthetic NDVI model. During model fitting, a random grid search was conducted with 250 iterations to identify the highest performing set of hyperparameters.

Model	Parameter Grid
GBM	'num_leaves': stats.randint(5,50), 'min_child_samples': stats.randint(10,30), 'boosting_type': ['gbdt', 'dart'], 'max_depth': stats.randint(5,25), 'n_estimators': [300, 400, 500]

Formatted: Normal

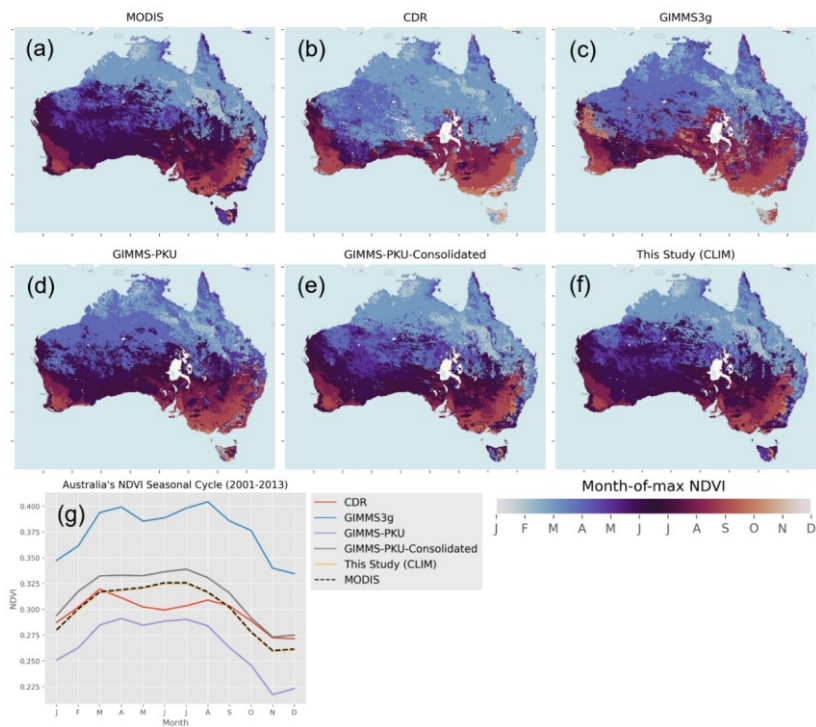


Figure A3: a-f) Month that maximum NDVI occurs, averaged from 2001-2013, for all NDVI datasets included in the intercomparison between NDVI products, along with the AusENDVI-clim dataset of this study. g) The climatological mean seasonal cycle of NDVI summarised over Australia.

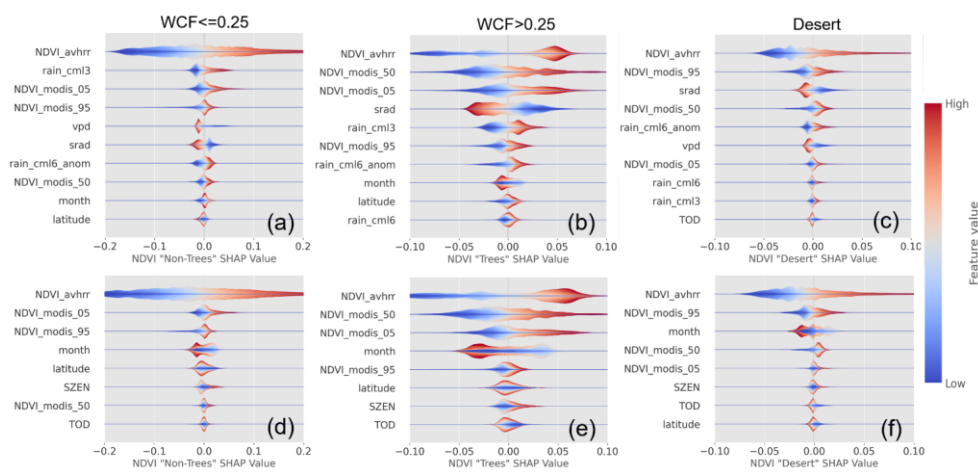
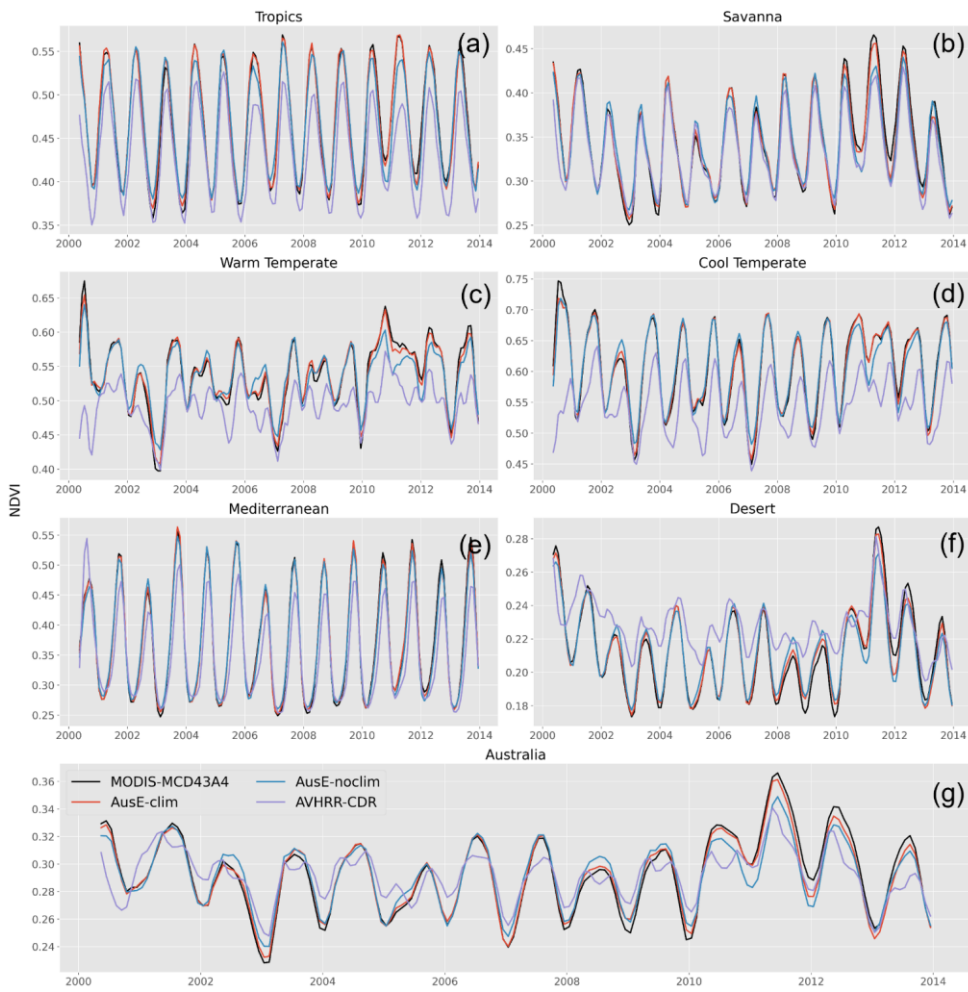
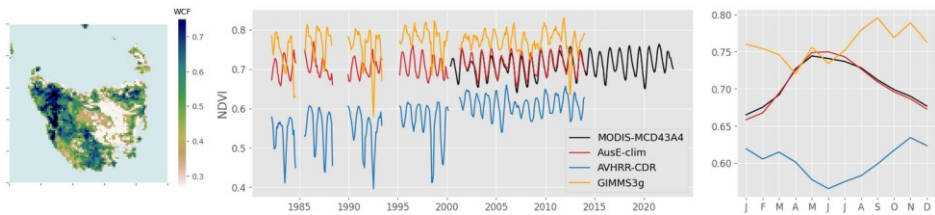


Figure A4: Feature importance plots for the calibration and harmonisation between $NDVI_{CDR}$ and $NDVI_{MCD43A4}$. a-c) show the results for the 'clim' model. d-f) shows the same but for the 'noclim' model type.



670

Figure A5: Per bioregion (a-f) and Australia-wide (g) NDVI time-series before and after the calibration and harmonisation of NDVI_{CDR}. Bioregions are defined in Figure 2b. Time series have been smoothed with a three-month rolling mean.

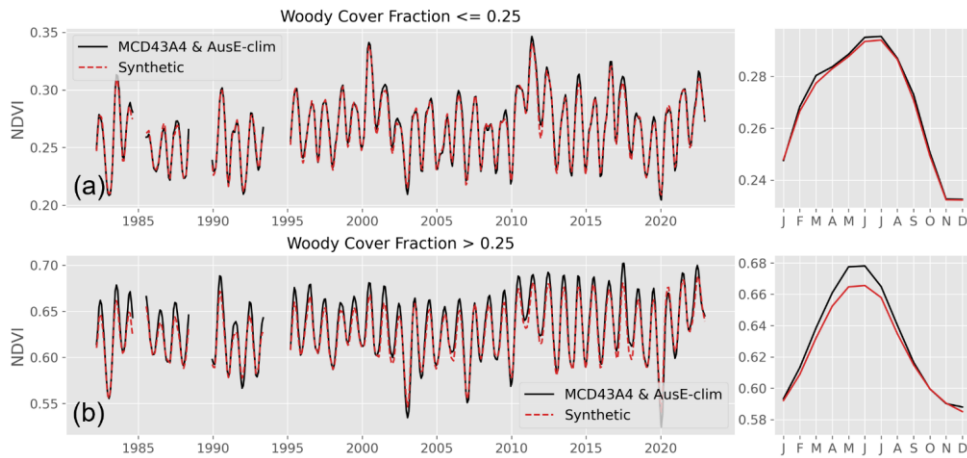


675 **Figure A6:** Same as Figure 6d-f but including $NDVI_{GIMMS3g}$ to demonstrate that the very strong increasing trend in $NDVI_{MCD43A4}$ is likely an artefact of sensor transitions and poor calibration.

Formatted: Subscript

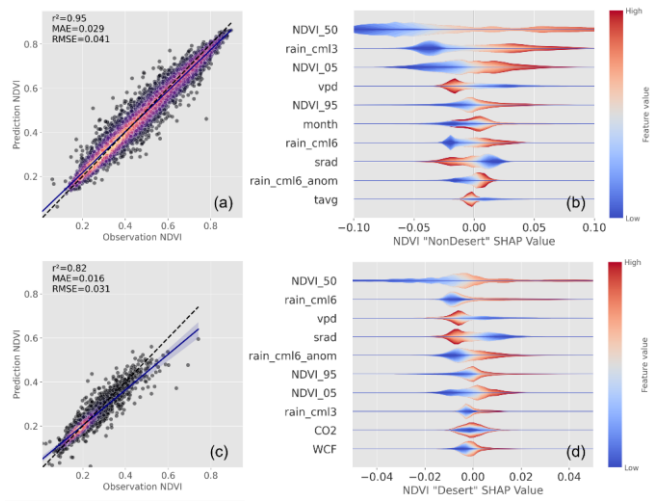
Formatted: Subscript

Formatted: Caption

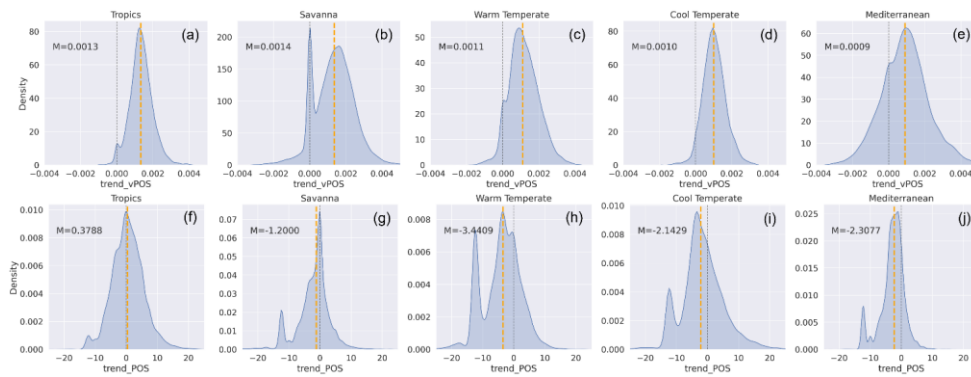


680 **Figure A7:** Evaluation of the synthetic NDVI built to gap fill $NDVI_{AusE-clim}$, disaggregated by high and low WCF regions. a) Spatially averaged observed and synthetic NDVI timeseries over all continental areas where WCF is less than or equal to 0.25. b) Same as (a) but for regions where WCF is greater than 0.25.

Formatted: Caption



685 **Figure A8: Validation scatter plots and feature importance plots for the gap-filling synthetic NDVI models. a-b) is for the ‘non-desert’ model region which covers the high and low woody cover regions shown in figure 1a, (c-d) is for the ‘desert’ region.**



690 **Figure A9: Distributions of pixel level trends in vPOS (a-e) and POS (f-j), summarised by bioclimatic region (excluding the desert region as most of this region is masked as non-seasonal). ‘M’ refers to the median slope value of the distribution and is indicated by the orange dashed line. Units for vPOS are NDVI per year and units for POS are days per decade.**

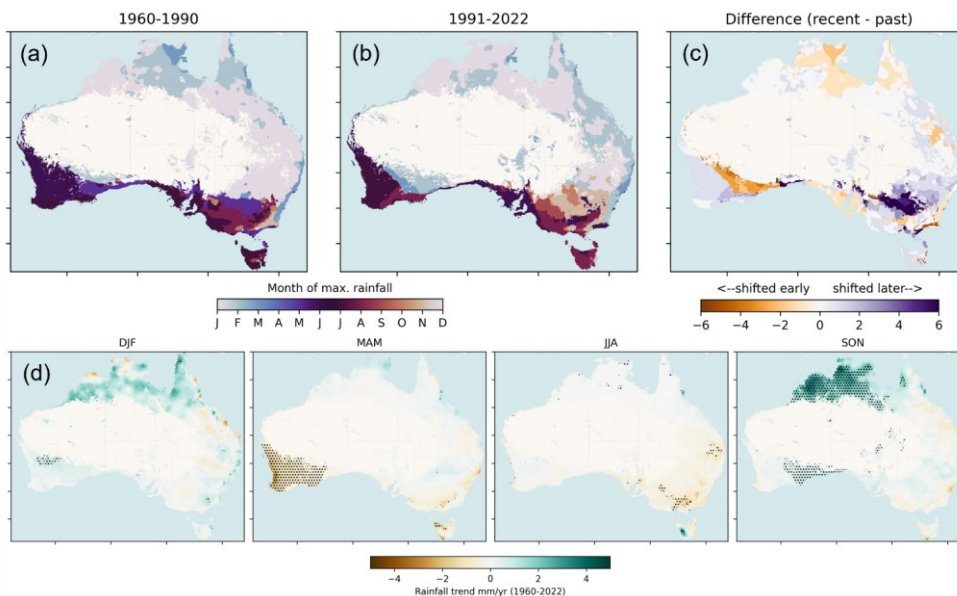


Figure A10: Changes to the timing and magnitude of rainfall in Australia. a) The typical month that rainfall achieves its maximum value, averaged from 1960-1990. b) Same as (a) but for a 1991-2022 climatology. c) The difference between (a) and (b) where the 1991-2022 climatology is subtracted from 1960-1990. Orange colours indicate earlier peak rainfall in the more recent climatology (in number of months). If peak rainfall shifts from January in 1960-1990 to December in 1991-2022, this is recorded as 'earlier' by one month. Purple colours indicate peak rainfall occurs later in 1991-2022 compared with 1960-1990. If peak rainfall shifts from December in 1960-1990 to January in 1991-2022, this is recorded as 'later' by one month. d) Theil-Sen trends in the total seasonal rainfall from 1960-2022. Hatching indicates significance at 95 % confidence using a Mann-Kendall test.

695

Author Contributions.

700 CB and SR conceived the study, CB performed all analysis and drafted the manuscript. SR, LR, and AVD provided extensive intellectual input and provided extensive edits to the manuscript.

Competing interests.

The authors declare that they have no conflicts of interest.

Acknowledgements

705 We thank the National Computing Infrastructure (NCI) for providing a research compute environment without which this work would not be possible.

Financial Support

The first author is supported by a research scholarship provided by Geoscience Australia, funded by the Australian Government.

710 References

- Beck, H. E., McVicar, T. R., van Dijk, A. I., Schellekens, J., de Jeu, R. A., and Bruijnzeel, L. A.: Global evaluation of four AVHRR–NDVI data sets: Intercomparison and assessment against Landsat imagery, *Remote Sensing of Environment*, 115, 2547-2563, 2011.
- Beringer, J., Moore, C. E., Cleverly, J., Campbell, D. I., Cleugh, H., De Kauwe, M. G., Kirschbaum, M. U., Griebel, A., Grover, S., and Huete, A.: Bridge to the future: Important lessons from 20 years of ecosystem observations made by the OzFlux network, *Global Change Biology*, 2022.
- 715 Bessenbacher, V., Seneviratne, S. I., and Gudmundsson, L.: CLIMFILL v0.9: a framework for intelligently gap filling Earth observations, *Geosci. Model Dev.*, 15, 4569-4596, 10.5194/gmd-15-4569-2022, 2022.
- Broich, M., Huete, A., Tulbure, M. G., Ma, X., Xin, Q., Paget, M., Restrepo-Coupe, N., Davies, K., Devadas, R., and Held, A.: Land surface phenological response to decadal climate variability across Australia using satellite remote sensing, *Biogeosciences*, 11, 5181-5198, 10.5194/bg-11-5181-2014, 2014.
- 720 Burton, C., Rifai, Sami, Renzullo, Luigi, & Van Dijk, Albert: AusENDVI: A long-term NDVI dataset for Australia (0.1.0) [dataset], <https://doi.org/10.5281/zenodo.10802704>, 2024.
- Byrne, G., Broomhall, M., Walsh, A. J., Thankappan, M., Hay, E., Li, F., McAtee, B., Garcia, R., Anstee, J., and Kerrisk, G.: Validating Digital Earth Australia NBART for the Landsat 9 Underfly of Landsat 8, *Remote Sensing*, 16, 1233, 2024.
- 725 Canadell, J. G., Meyer, C., Cook, G. D., Dowdy, A., Briggs, P. R., Knauer, J., Pepler, A., and Haverd, V.: Multi-decadal increase of forest burned area in Australia is linked to climate change, *Nature communications*, 12, 6921, 2021.
- Cawley, G. C. and Talbot, N. L.: On over-fitting in model selection and subsequent selection bias in performance evaluation, *The Journal of Machine Learning Research*, 11, 2079-2107, 2010.
- 730 Chambers, L. E., Altwegg, R., Barbraud, C., Barnard, P., Beaumont, L. J., Crawford, R. J., Durant, J. M., Hughes, L., Keatley, M. R., and Low, M.: Phenological changes in the southern hemisphere, *PloS one*, 8, e75514, 2013.
- Chen, B.: Comparison of the Two Most Common Phenology Algorithms Imbedded in Land Surface Models, *Journal of Geophysical Research: Atmospheres*, 127, e2022JD037167, 2022.
- Cortés, J., Mahecha, M. D., Reichstein, M., Myneni, R. B., Chen, C., and Brenning, A.: Where are global vegetation greening and browning trends significant?, *Geophysical Research Letters*, 48, e2020GL091496, 2021.
- 735 Donohue, R. J., McVICAR, T. R., and Roderick, M. L.: Climate-related trends in Australian vegetation cover as inferred from satellite observations, 1981–2006, *Global Change Biology*, 15, 1025-1039, 2009.
- Donohue, R. J., Roderick, M. L., McVicar, T. R., and Farquhar, G. D.: Impact of CO2 fertilization on maximum foliage cover across the globe's warm, arid environments, *Geophysical Research Letters*, 40, 3031-3035, 2013.
- Dusenge, M. E., Duarte, A. G., and Way, D. A.: Plant carbon metabolism and climate change: elevated CO2 and temperature impacts on photosynthesis, photorespiration and respiration, *New Phytologist*, 221, 32-49, 2019.
- 740 Fensholt, R. and Proud, S. R.: Evaluation of earth observation based global long term vegetation trends—Comparing GIMMS and MODIS global NDVI time series, *Remote sensing of Environment*, 119, 131-147, 2012.
- Franch, B., Vermote, E. F., Roger, J.-C., Murphy, E., Becker-Reshef, I., Justice, C., Claverie, M., Nagol, J., Csaszar, I., and Meyer, D.: A 30+ year AVHRR land surface reflectance climate data record and its application to wheat yield monitoring, *Remote Sensing*, 9, 296, 2017.

745 Frankenberg, C., Yin, Y., Byrne, B., He, L., and Gentine, P.: Comment on “Recent global decline of CO₂ fertilization effects on vegetation photosynthesis”, *Science*, 373, eabg2947, 2021.

Gerber, F., de Jong, R., Schaepman, M. E., Schaepman-Strub, G., and Furrer, R.: Predicting missing values in spatio-temporal remote sensing data, *IEEE Transactions on Geoscience and Remote Sensing*, 56, 2841-2853, 2018.

750 Giglio, L. and Roy, D.: On the outstanding need for a long-term, multi-decadal, validated and quality assessed record of global burned area: Caution in the use of Advanced Very High Resolution Radiometer data, *Science of Remote Sensing*, 2, 100007, 2020.

Gorman, A. and McGregor, J.: Some considerations for using AVHRR data in climatological studies: II. Instrument performance, *REMOTE SENSING*, 15, 549-565, 1994.

755 Haverd, V., Raupach, M. R., Briggs, P. R., Canadell, J. G., Isaac, P., Pickett-Heaps, C., Roxburgh, S. H., van Gorsel, E., Viscarra Rossel, R. A., and Wang, Z.: Multiple observation types reduce uncertainty in Australia's terrestrial carbon and water cycles, *Biogeosciences*, 10, 2011-2040, 10.5194/bg-10-2011-2013, 2013.

Head, L., Adams, M., McGregor, H. V., and Toole, S.: Climate change and Australia, *Wiley Interdisciplinary Reviews: Climate Change*, 5, 175-197, 2014.

Hoffmann, A. A., Rymper, P. D., Byrne, M., Ruthrof, K. X., Whinam, J., McGeoch, M., Bergstrom, D. M., Guerin, G. R., Sparrow, B., and Joseph, L.: Impacts of recent climate change on terrestrial flora and fauna: Some emerging Australian examples, *Austral Ecology*, 44, 3-27, 2019.

760 Hope, P. K., Drosowsky, W., and Nicholls, N.: Shifts in the synoptic systems influencing southwest Western Australia, *Climate Dynamics*, 26, 751-764, 2006.

Hopper, S. D. and Gioia, P.: The southwest Australian floristic region: evolution and conservation of a global hot spot of biodiversity, *Annu. Rev. Ecol. Evol. Syst.*, 35, 623-650, 2004.

765 Huang, Z., Zhou, L., and Chi, Y.: Spring phenology rather than climate dominates the trends in peak of growing season in the Northern Hemisphere, *Global Change Biology*, 2023.

Hughes, L.: Climate change and Australia: key vulnerable regions, *Regional Environmental Change*, 11, 189-195, 2011.

Hutchison, M., Kesteven, J., and Xu, T.: ANUclimate collection [dataset], 2014.

770 Krause, C., Dunn, B., Bishop-Taylor, R., Adams, C., Burton, C., Alger, M., Chua, S., Phillips, C., Newey, V., and Kouzoubov, K.: Digital Earth Australia notebooks and tools repository, *Geoscience Australia*, 2021.

Li, F., Jupp, D. L., Reddy, S., Lymburner, L., Mueller, N., Tan, P., and Islam, A.: An evaluation of the use of atmospheric and BRDF correction to standardize Landsat data, *IEEE Journal of Selected Topics in Applied Earth Observations and Remote Sensing*, 3, 257-270, 2010.

775 Li, M., Cao, S., Zhu, Z., Wang, Z., Myneni, R. B., and Piao, S.: Spatiotemporally consistent global dataset of the GIMMS Normalized Difference Vegetation Index (PKU GIMMS NDVI) from 1982 to 2022, *Earth Syst. Sci. Data*, 15, 4181-4203, 10.5194/essd-15-4181-2023, 2023.

Liao, Z., Van Dijk, A. I., He, B., Larraondo, P. R., and Search, P. F.: Woody vegetation cover, height and biomass at 25-m resolution across Australia derived from multiple site, airborne and satellite observations, *International Journal of Applied Earth Observation and Geoinformation*, 93, 102209, 2020.

780 Liu, Y., Wu, C., Wang, X., Jassal, R. S., and Gonsamo, A.: Impacts of global change on peak vegetation growth and its timing in terrestrial ecosystems of the continental US, *Global and Planetary Change*, 207, 103657, 2021.

Lundberg, S. M. and Lee, S.-I.: A unified approach to interpreting model predictions, *Advances in neural information processing systems*, 30, 2017.

785 Ma, X., Huete, A., and Tran, N. N.: Interaction of seasonal sun-angle and savanna phenology observed and modelled using MODIS, *Remote Sensing*, 11, 1398, 2019.

Ma, X., Huete, A., Moran, S., Ponce-Campos, G., and Eamus, D.: Abrupt shifts in phenology and vegetation productivity under climate extremes, *Journal of Geophysical Research: Biogeosciences*, 120, 2036-2052, 2015.

790 Ma, X., Huete, A., Yu, Q., Coupe, N. R., Davies, K., Broich, M., Ratana, P., Beringer, J., Hutley, L. B., and Cleverly, J.: Spatial patterns and temporal dynamics in savanna vegetation phenology across the North Australian Tropical Transect, *Remote sensing of Environment*, 139, 97-115, 2013.

Meyer, H. and Pebesma, E.: Machine learning-based global maps of ecological variables and the challenge of assessing them, *Nature Communications*, 13, 1-4, 2022.

795 Moore, C. E., Brown, T., Keenan, T. F., Duursma, R. A., van Dijk, A. I. J. M., Beringer, J., Culvenor, D., Evans, B., Huete, A., Hutley, L. B., Maier, S., Restrepo-Coupe, N., Sonntag, O., Specht, A., Taylor, J. R., van Gorsel, E., and Liddell, M. J.: Reviews and syntheses: Australian vegetation phenology: new insights from satellite remote sensing and digital repeat photography, *Biogeosciences*, 13, 5085-5102, 10.5194/bg-13-5085-2016, 2016.

Myers, N., Mittermeier, R. A., Mittermeier, C. G., Da Fonseca, G. A., and Kent, J.: Biodiversity hotspots for conservation priorities, *Nature*, 403, 853-858, 2000.

800 O'Donnell, J., Gallagher, R. V., Wilson, P. D., Downey, P. O., Hughes, L., and Leishman, M. R.: Invasion hotspots for non-native plants in a ustralia under current and future climates, *Global Change Biology*, 18, 617-629, 2012.

- Park, T., Chen, C., Macias-Fauria, M., Tømmervik, H., Choi, S., Winkler, A., Bhatt, U. S., Walker, D. A., Piao, S., and Brovkin, V.: Changes in timing of seasonal peak photosynthetic activity in northern ecosystems, *Global change biology*, 25, 2382-2395, 2019.
- Peters, J. M., López, R., Nolf, M., Hutley, L. B., Wardlaw, T., Cernusak, L. A., and Choat, B.: Living on the edge: A continental-scale assessment of forest vulnerability to drought, *Global Change Biology*, 27, 3620-3641, 2021.
- 805 Piao, S., Liu, Q., Chen, A., Janssens, I. A., Fu, Y., Dai, J., Liu, L., Lian, X., Shen, M., and Zhu, X.: Plant phenology and global climate change: Current progresses and challenges, *Global change biology*, 25, 1922-1940, 2019.
- Pinzon, J. E. and Tucker, C. J.: A non-stationary 1981–2012 AVHRR NDVI3g time series, *Remote sensing*, 6, 6929-6960, 2014.
- Pitman, A., Narisma, G., Pielke Sr, R., and Holbrook, N.: Impact of land cover change on the climate of southwest Western Australia, *Journal of Geophysical Research: Atmospheres*, 109, 2004.
- 810 Poulter, B., Frank, D., Ciais, P., Myneni, R. B., Andela, N., Bi, J., Broquet, G., Canadell, J. G., Chevallier, F., and Liu, Y. Y.: Contribution of semi-arid ecosystems to interannual variability of the global carbon cycle, *Nature*, 509, 600-603, 2014.
- Privette, J., Fowler, C., Wick, G., Baldwin, D., and Emery, W.: Effects of orbital drift on AVHRR products: normalized difference vegetation index and sea surface temperature, *Remote Sens. Environ.*, 53, 164-177, 1995.
- Rifai, S. W., De Kauwe, M. G., Ukkola, A. M., Cernusak, L. A., Meir, P., Medlyn, B. E., and Pitman, A. J.: Thirty-eight years of CO2 fertilization has outpaced growing aridity to drive greening of Australian woody ecosystems, *Biogeosciences*, 19, 491-515, 10.5194/bg-19-491-2022, 2022.
- 815 Schaaf, C. and Wang, Z.: MCD43A4 MODIS/Terra+ aqua BRDF/albedo nadir BRDF adjusted RefDaily L3 global 500 m V006, NASA EOSDIS Land Processes DAAC, 2015.
- Shen, H., Li, X., Cheng, Q., Zeng, C., Yang, G., Li, H., and Zhang, L.: Missing information reconstruction of remote sensing data: A technical review, *IEEE Geoscience and Remote Sensing Magazine*, 3, 61-85, 2015.
- 820 Steffen, W., Sims, J., Walcott, J., and Laughlin, G.: Australian agriculture: coping with dangerous climate change, *Regional Environmental Change*, 11, 205-214, 2011.
- Tian, F., Fensholt, R., Verbesselt, J., Grogan, K., Horion, S., and Wang, Y.: Evaluating temporal consistency of long-term global NDVI datasets for trend analysis, *Remote Sensing of Environment*, 163, 326-340, 2015.
- 825 Tucker, C. J., Pinzon, J. E., Brown, M. E., Slayback, D. A., Pak, E. W., Mahoney, R., Vermote, E. F., and El Saleous, N.: An extended AVHRR 8-km NDVI dataset compatible with MODIS and SPOT vegetation NDVI data, *International journal of remote sensing*, 26, 4485-4498, 2005.
- Ukkola, A. M., Prentice, I. C., Keenan, T. F., Van Dijk, A. I., Viney, N. R., Myneni, R. B., and Bi, J.: Reduced streamflow in water-stressed climates consistent with CO2 effects on vegetation, *Nature Climate Change*, 6, 75-78, 2016.
- 830 Vermote, E. F., El Saleous, N. Z., and Justice, C. O.: Atmospheric correction of MODIS data in the visible to middle infrared: first results, *Remote Sensing of Environment*, 83, 97-111, 2002.
- Wang, S., Zhang, Y., Ju, W., Chen, J. M., Cescatti, A., Sardans, J., Janssens, I. A., Wu, M., Berry, J. A., and Campbell, J. E.: Response to Comments on "Recent global decline of CO2 fertilization effects on vegetation photosynthesis", *Science*, 373, eabg7484, 2021.
- 835 Wang, Z., Wang, H., Wang, T., Wang, L., Liu, X., Zheng, K., and Huang, X.: Large discrepancies of global greening: Indication of multi-source remote sensing data, *Global Ecology and Conservation*, 34, e02016, 2022.
- Xie, Q., Moore, C. E., Cleverly, J., Hall, C. C., Ding, Y., Ma, X., Leigh, A., and Huete, A.: Land surface phenology indicators retrieved across diverse ecosystems using a modified threshold algorithm, *Ecological Indicators*, 147, 110000, 2023.
- Ye, W., van Dijk, A. I., Huete, A., and Yebra, M.: Global trends in vegetation seasonality in the GIMMS NDVI3g and their robustness, *International Journal of Applied Earth Observation and Geoinformation*, 94, 102238, 2021.
- 840 Zeng, C., Shen, H., Zhong, M., Zhang, L., and Wu, P.: Reconstructing MODIS LST based on multitemporal classification and robust regression, *IEEE Geoscience and Remote Sensing Letters*, 12, 512-516, 2014.